Cellular reconstitution of apoptotic cell clearance reveals a multi-step phosphorylation mechanism for Draper receptor triggering

Adam P. Williamson[1, 2] and Ronald D. Vale[1, 2*]

[1]Dept. of Cellular and Molecular Pharmacology and the [2]Howard Hughes Medical Institute, University of California, San Francisco, CA 94158

[*]Address correspondence to: ron.vale@ucsf.edu

Summary

Apoptotic cells are cleared after exposing “eat me” ligands, including phosphatidylserine (PS), but the signaling pathway in the phagocytic cell that leads to engulfment remains poorly understood. Here, by transfecting the engulfment receptor Draper into Drosophila S2 cells and using PS-coated beads to mimic apoptotic cells, we have created a simplified system for studying this process. We show that ligand-bound Draper forms mobile microclusters that recruit effector proteins and exclude a transmembrane phosphatase, suggesting a kinetic segregation mechanism for receptor activation similar to T cell receptors. Like the TCR, Draper’s extracellular domain and ligand can be replaced with other interacting modules. We show that phosphorylation of Draper’s ITAM motif occurs first and is a dominant contributor to signaling. After ITAM phosphorylation, additional residues become phosphorylated and contribute to signaling efficiency. Our results demonstrate broad mechanistic similarities between Draper and mammalian immune receptor activation and an ability to reprogram engulfment signaling.

Keywords: Signaling, phagocytosis, cell engulfment, corpse clearance, efferocytosis, apoptosis, phosphatidylserine, *Drosophila*, Draper, Shark

Introduction

The prompt clearance of dying cells and debris is essential for maintaining homeostasis and promoting tissue repair (Arandjelovic and Ravichandran, 2015; Neumann et al., 2015; Reddien and Horvitz, 2004). In healthy tissue, resident and infiltrating phagocytes clear cell corpses and debris through specific recognition, uptake, and digestion (Elliott and Ravichandran, 2010). Defects in clearance result in autoimmunity and further tissue damage (Elliott and Ravichandran, 2010; Iram et al., 2016). Despite the importance of efficient clearance across multicellular life, our understanding of the underlying mechanism remains poorly understood in comparison to other signaling systems. Important questions about how an apoptotic corpse triggers its clearance by professional phagocytic cells remain unanswered. Developing a better understanding of this process could lead to new strategies of enhancing clearance under conditions of extreme injury or enabling engulfment of choice targets such as cancer cells.

Apoptotic cell clearance requires a complex signaling network triggered by interactions between receptors on the phagocyte and ligands exposed on the dying cells. These “eat me” signals trigger cytosolic signaling that ultimately promotes cytoskeletal rearrangements that power corpse internalization (Ravichandran and Lorenz, 2007; Reddien and Horvitz, 2004). Phagocytes express receptors that recognize distinct ligands either directly or through bridging molecules (S. A. Freeman and Grinstein, 2014; Penberthy and Ravichandran, 2016). Although the basic mechanics of clearance are likely conserved across metazoans, the receptors and ligands are diverse. Perhaps as a consequence of this molecular diversity, the biochemical and biophysical triggers of phagocytic receptor activation and the downstream consequences of triggering remain unclear. Important open questions include: How do apoptotic ligands cause the phosphorylation of receptor cytosolic tails? How do ligated receptors organize themselves on plasma membranes? How are cytosolic effectors recruited to receptors?

Draper is a Drosophila receptor that is expressed in glia, where it promotes clearance of damaged axons, and in the somatic epithelium, where it functions to remove dying cells from the follicle (Etchegaray et al., 2012; M. R. Freeman et al., 2003; MacDonald et al., 2006). Draper is similar in domain structure to the mammalian protein Megf10 and CED-1, the first described apoptotic corpse receptor in C. elegans. All three receptors contain single pass transmembrane domains that connect extracellular EGF repeats to intracellular tyrosine phosphorylation sites that are presumed to recruit one or more downstream effectors (Scheib et al., 2012; Zhou et al., 2001; Ziegenfuss et al., 2008). Draper function has been dissected genetically, especially in its damaged axon clearance role, which defined a “parts list” of other proteins involved in engulfment signaling, including the kinases Src42a and Shark and the adapter protein Crk (Lu et al., 2014; Ziegenfuss et al., 2008; 2012). However, biochemical interactions are less well understood, and how these molecules work together to promote clearance remains an open question. In particular, our understanding of Draper phosphorylation and the immediate downstream events is poor.

A clue to the mechanism of Draper activity comes from the recognition that its sequence bears an Immune Tyrosine Activation Motif (ITAM) domain that is found in several copies in the T cell receptor, a receptor that evolved in vertebrates with an adaptive immune system (Schultz et al., 2000; Zhou et al., 2001; Ziegenfuss et al., 2008). Furthermore, Shark, an important kinase in the engulfment signaling pathway uncovered through genetics, bears domain and sequence identify to ZAP70 and Syk, tyrosine kinases involved in immune responses which bind directly to doubly-phosphorylated tyrosines in the ITAM domain (Ziegenfuss et al., 2008). A subset of molecules implicated in Draper signaling (e.g. Crk) also contain SH2 and SH3 domains that bear some similarity to multivalent adapters such as Grb2 and Gads that function in mammalian immune signaling and other systems (Choudhuri and Dustin, 2010). While these genetic and

sequence level clues are tantalizing, evidence showing that Draper has functional parallels with mammalian adaptive immune signaling is lacking. Understanding both the functional similarities and differences between Draper and adaptive immune receptor signaling could provide important clues into the mechanism of phagocytosis.

Here, we have reconstituted Draper-mediated signaling in Drosophila S2 cells to understand how this receptor triggers phagocytosis. We find that Draper ligation to the lipid phosphatidylserine (PS) incorporated into supported lipid bilayers is sufficient to induce its phosphorylation and a signaling cascade leading to engulfment. Like the TCR, ligated Draper forms mobile microclusters that shift a kinase-phosphatase balance toward receptor phosphorylation and the recruitment of downstream effector proteins. We also reveal other mechanistic parallels between Draper signaling and T cell signaling, including the ability to replace the extracellular module of Draper and PS with an inducible artificial receptor-ligand interaction. Unlike the TCR, where the ITAM phosphorylation domain is sufficient for signaling, we show that full activation of Draper requires an initial ITAM phosphorylation followed by the phosphorylation of other tyrosines in its tail domain. The reconstitution and reprogramming of Draper signaling reveals how distinct modules in the receptor work in concert to promote signaling and uncovers new insight into functional similarities and differences between phagocytic and mammalian adaptive immune signaling systems.

Results

Cellular reconstitution of Draper signaling

We used cultured Drosophila S2 cells, which are derived from a hemocyte lineage (Schneider, 1972), as a cellular system for reconstituting phagocytosis. Drosophila S2 cells display a very low level of engulfment of cell corpses (Fig. 1A), which were prepared by inducing apoptosis in S2 cells by addition of 1 μM actinomycin for 16 hr. We hypothesized that the level of engulfment might be low because S2 cells lack sufficient levels of engulfment receptors. Consistent with this idea Draper, the best known engulfment receptor in Drosophila, is expressed at low levels in S2 cells as measured by RNA-Seq (Cherbas et al., 2011). Fluorescently-labeled corpses were then added to cultures of either Draper- or control mCherry-transfected S2 cells and, after 45 min, the presence of internalized annexinV-647-labeled corpses was scored. Our results revealed that Draper transfection increased the uptake of apoptotic cell corpses by ~5 fold (Fig. 1A).

Apoptotic cells express an array of “eat me” ligands (Ravichandran and Lorenz, 2007). As a next step, we sought to provide a simplified target of uniform size. The lipid phosphatidylserine (PS) is exposed on dying cells and is considered to be an important “eat me” signal (Fadok et al., 1992). PS was proposed to be a Draper activator (Tung et al., 2013), but a protein ligand for Draper has also been suggested (Kuraishi et al., 2009). It has not been established whether PS is necessary and sufficient for Draper-mediated engulfment. To determine if PS alone might suffice for Draper-mediated engulfment, we replaced the apoptotic cells with 6.5 micron diameter silica beads coated with a supported lipid bilayer (SLB) containing 10% PS and 0.5% atto390-PE lipid for visualization by microscopy (Fig. 1B). Draper-GFP S2 cells engulfed ~0.8 PS beads/cell, on average, after a 30 min incubation (Fig. 1B), which was 50-fold higher than

the ingestion of beads coated only with PC alone. Control GFP S2 cells also engulfed PS-coated beads ~7 fold less efficiently than the Draper-GFP transfected cells, (Fig. 1B). Draper-GFP S2 cells engulfed beads at 2.5% PS lipid content and showed increasing engulfment up to 12.5% PS (Fig. 1C). The PS concentrations that promote engulfment of beads are within the physiological range present on dead and dying cells (Leventis and Grinstein, 2010). Thus, our S2 cell system represents a simplified engulfment assay that is dependent on 1) overexpression of the Draper receptor, and 2) PS exposed on a SLB-coated bead. Importantly, these results also demonstrate that PS is a functional ligand for Draper and is necessary and sufficient for Draper-mediated engulfment.

We next performed live cell microscopy to visualize the process of Draper-mediated engulfment of PS beads (stills Fig. 1D, Movie 1). We co-transfected Draper-mCherry and LifeAct-GFP in S2 cells and imaged PS bead engulfment by time-lapse imaging. Draper-mCherry expressing cells formed a synapse with PS beads and rapidly began forming a phagocytic cup; F-actin, as assessed by LifeAct-GFP signal, localized at the edges of the cup and the leading edge of the cup extended gradually around the bead. When the phagocytic cup was complete, the PS bead was internalized. Thus, our system is useful for determining the kinetics of PS bead engulfment and following the dynamics of the cytoskeleton and membranes downstream of Draper activation.

Draper ligation nucleates the formation of mobile microclusters enriched in phosphotyrosine and phosphotyrosine-binding proteins

After engaging with damaged axon, Draper expressed in glial cells becomes tyrosine phosphorylated, which then enables it to recruit a Syk-related related tyrosine kinase called Shark (Ziegenfuss et al., 2008). After incubating Draper-GFP S2 cells with 10% PS beads, we

found a strong pTyr signal at the plasma membrane at the interface between Draper-GFP S2 cell and the PS bead, which diminished after internalization (Fig. 2A). Consistent with the studies of Ziegenfuss et al. (2008), we also found that Shark-mCherry co-localized with Draper-GFP at the interface between PS bead and the Draper-transfected S2 cell (Fig. 2B).

To better visualize the behavior of Draper and the recruitment of proteins to the plasma membrane, we developed a signaling system that is compatible with Total Internal Reflection Fluorescence-Microscopy (TIRF-M), a technique that confines illumination to within ~200 nm of the glass coverslip. Instead of using a bead, we coated the glass coverslip with a supported lipid bilayer contain 10% PS (Fig 2C). When Draper-GFP S2 cells settled on this PS supported lipid bilayer, the cells spread rapidly on the surface in a futile effort to engulf the planar surface. Strikingly, Draper-GFP organized in microclusters that underwent retrograde flow from the leading edge towards a central synapse (Fig. 2D; Movie 2). The behavior of these Draper clusters is very similar to that reported for adaptive immune receptor clusters that form in B and T cells (Kaizuka et al., 2007; Murugesan et al., 2016). To determine if Draper clusters have local effects on the actin cytoskeleton, we co-expressed Draper-GFP and LifeAct-BFP and allowed these cells to settle on PS bilayers. Draper-GFP microclusters appeared at the SLB interface with LifeAct-BFP; as the clusters grew, LifeAct-BFP signal was depleted (Movie 3). The central synapse was depleted of F-actin, as imaged by LifeAct-BFP. Thus, Draper activation at the plasma membrane leads to clusters that undergo retrograde flow and correlates with local actin cytoskeleton remodeling.

Next, we asked if Draper-GFP clusters are sites of recruitment for downstream signaling molecules. Draper is proposed to interact with Shark, a dual SH2 protein, and an adapter Crk, which harbors one SH2 and two SH3 domains. To test if these proteins are recruited to Draper microclusters, we allowed Draper-GFP, Shark-TagBFP, Crk-mCherry transfected S2 cells to

settle on 10% PS bilayers and then imaged them by TIRF microscopy. Draper-GFP microclusters co-localized with Shark-TagBFP and Crk-mCherry (Fig. 2E, Movie 4), indicating that Draper-GFP microclusters, like TCR microclusters, recruit a tandem SH2-domain containing kinase and an adapter protein to the plasma membrane. Crk and the activating subunit of the PI3K p85 also co-localize at the synapse between PS bead and Draper-expressing S2 cell, indicating that Draper may organize multiple signaling outputs (Fig. S1). Our results demonstrate that upon ligation to PS, Draper is phosphorylated and nucleates formation of signaling microclusters that recruit SH2-domain containing proteins.

Exclusion of a transmembrane phosphatase at the ligated membrane-membrane interface

We next used our reconstitution system to understand the mechanism of how PS triggers Draper phosphorylation. The T cell receptor is believed to be triggered by the exclusion of the transmembrane phosphatase CD45, which has a bulky extracellular domain, from zones of close membrane-membrane contact created by the pMHC-TCR interaction (Burroughs et al., 2006; Choudhuri et al., 2005; James and Vale, 2012). Since the Src family kinase Lck is attached to the membrane inner leaflet and remains uniformly distributed after pMHC-TCR engagement, phosphatase exclusion shifts the kinase-phosphatase balance towards net receptor phosphorylation. We sought to test whether a similar mechanism might function to trigger Draper phosphorylation. Drosophila S2 cells expresses several transmembrane phosphatases (Fig. S2A). We tested the transmembrane phosphatase Ptp69D, because of its high expression and similar domain structure to CD45 (extracellular fibronectin repeats and cytosolic tyrosine phosphatase activity (Fig. S2B)). To determine if Draper clusters are segregated from Ptp69D, we co-transfected the two proteins with different fluorescent protein tags and assessed localization during Draper ligation in living cells. Microscopy revealed that

ligated Draper-mCherry concentrated at the synapse between the S2 cell and PS bead, while Ptp69D-GFP was partially excluded from this zone (Fig. 3A). Draper microclusters that formed at the interface between an S2 cell and a PS-containing supported lipid bilayer also excluded Ptp69D (Fig. S2C). Thus, ligated Draper is able to segregate away from an abundant transmembrane phosphatase, a result that is consistent with a kinetic segregation triggering mechanism.

In the kinetic segregation model, two opposing membranes are brought into close apposition by the binding energy between receptor and its ligand, which results in the exclusion of larger transmembrane phosphatases. To further examine whether Draper may trigger phosphorylation through a kinetic segregation mechanism rather than a receptor conformational change, we tested whether the extracellular domain of Draper and its ligand PS could be replaced with an artificial receptor-ligand pair. Previous studies on the T cell receptor triggering showed that the extracellular domain of the TCR and pMHC could be substituted with FKBP and FRB, which upon addition of rapamycin to bridge FKBP and FRB, would trigger TCR phosphorylation (James and Vale, 2012). We created a similar inducible system for Draper by replacing its extracellular domain with FRB (FRB-EXT-Draper-INT) and replacing PS with His_{10}-FKBP, which was bound to the SLB on the bead via a NiNTA-lipid (Fig 3B). In the absence of rapamycin, beads were engulfed at very low levels (0.003 beads/cell). However, in the presence of rapamycin, the engineered receptor promoted robust engulfment of FKBP-bearing beads (Fig. 3C, Movie 5). Live cell microscopy revealed that the FRB-EXT-Draper-INT concentrated at the cell-bead interface and recruited Shark kinase, suggesting that the chimeric receptor, like Draper, is activated by tyrosine phosphorylation (Fig 3D). When His_{10}-FKBP was attached to a SLB on a coverslip, the cells spread on the surface. Like Draper-GFP, FRB-EXT-Draper-INT excluded the phosphatase Ptp69D-GFP (Fig. 3E), consistent with a kinetic segregation-based

triggering mechanism. Thus a chimeric receptor that is designed to interact with a non-physiological ligand is functional for engulfment.

Roles of Draper's cytoplasmic Tyr residues for engulfment of PS beads

We next sought to determine which Tyr residues are essential for full Draper activity. The Draper tail domain contains an ITAM motif (YxxI/Lx_{6-12}YxxI/L), an NPxY motif thought to interact CED-6 (Fujita et al., 2012), and 10 other tyrosine residues, 2 of which are in close proximity to the transmembrane domain. First, we created a construct in which 11 of the 13 tyrosines were mutated to alanine, leaving the two tyrosines that are immediately adjacent to the transmembrane segment since they potentially could have a structural role. We then compared phagocytic proficiency of cells transfected with Draper-Ala11-GFP mutant to full-length Draper-GFP and GFP alone control (endogenous background phagocytosis). Consistent with a role for Tyr phosphorylation on Draper to promote phagocytosis, Draper-Ala11-GFP ingested PS-beads at levels that were comparable to the GFP control and ~15-fold below Draper-GFP cells after a 45 min incubation (Fig 4A).

Genetic studies in Drosophila indicated at Shark kinase is involved in Draper signaling (Ziegenfuss et al., 2008), but the Draper ITAM, which recruits Shark, is also important for other aspects of Draper function including migration to sites of damage (Evans et al., 2015). To test the roles of the ITAM in our system, we mutated the 2 Tyr residues in the ITAM to Phe (Draper-ΔITAM; residues in 4B) and assessed its ability to promote phagocytosis. Draper-ΔITAM showed a kinetic delay and a lower number of beads ingested (Figure 4C) compared to wildtype Draper, although, it still promoted phagocytosis to a greater extent than the effectively null Draper-Ala11 construct.

We also tested if Draper's ITAM is sufficient to signal by adding back the ITAM tyrosines (Y934 and Y949) to the null Ala-11 mutant. The Draper ITAM Only receptor promoted phagocytosis of PS beads, but did so more slowly than wildtype and to a lesser extent than wildtype Draper. As expected, the Draper ITAM was necessary and sufficient to recruit Shark kinase to the synapse between S2 cell and PS bead (Fig. S3). Collectively, our mutational analyses suggest that both Draper's ITAM plays a major role in signaling but that non-ITAM residues also contribute to full receptor activity in engulfing PS beads.

Hierarchical multi-site Tyr phosphorylation in vitro

Using a biochemical system with purified components, we sought to test the role of the Draper's ITAM domain on Shark binding and receptor phosphorylation. To detect binding between Shark and Draper, we used a fluorescently-labeled tandem SH2 Shark construct (BG505-tSH2-Shark) whose signal quenches upon binding to liposome-bound Draper (Hui and Vale, 2014) (schematic Fig. 5A). With Src42a in solution and ATP added to trigger phosphorylation, we observed a time-dependent quenching of Shark fluorescence as it bound to the phosphorylated receptor (Fig. 5A, orange trace). Next we tested the Draper receptor with double tyrosine mutation in its ITAM motif (Draper-ΔITAM). Draper-ΔITAM showed little or no recruitment of Shark (Fig. 5A, blue trace).

Next, we tested the extent and order of Tyr phosphorylation events on Draper's cytoplasmic tail in this biochemical assay. After a 30 min kinase reaction, immunoblotting with anti-phosphotyrosine antibodies revealed a noticeable shift in the electrophoretic mobility of Draper, which is suggestive of phosphorylation on multiple Tyr residues (Fig. 5B). Remarkably, even though the Draper Y934F/Y949F mutant contains 9 additional tyrosine residues, its

phosphorylation as detected by phosphotyrosine immunoblotting was minimal (5% of wildtype Draper) in the same kinase reaction (Fig. 5B).

This result greatly diminished phosphorylation of the Draper Y934F/Y949F mutant could be due to 1) only the ITAM domains are phosphorylated by Src42a, or 2) or that phosphorylation of the ITAM motif is needed for the phosphorylation of non-ITAM in Draper's tail. To distinguish between these possibilities, we performed 1D mass spectrometry. After a 4 min incubation with Src42a, we observed that the first ITAM tyrosine (Y934) was phosphorylated; phosphorylation on the second ITAM residue Y949 was not detected but the Y949 containing peptide was not highly covered in our mass spec (Fig. 5C). In addition to Y934, we found several other residues that were phosphorylated (Y858, Y888, Y901, Y905, and Y925). This result indicates that the ITAM is not only target for Src42a. Src42a is the most likely candidate for Draper phosphorylation based upon genetic studies (Ziegenfuss et al., 2008). However, we also wanted to establish whether other Src family kinases behave in a similar way to Src42a with respect to Draper phosphorylation. We tested Lck, a well-studied Src family kinase in immune cells. Like Src42a, Lck readily phosphorylated Draper on Y888, Y901, Y905, Y925, and the Y934 ITAM residue (but not Y858)(Figure S4). Similar to results with Src42a, for the Draper Y934F/Y949F mutant, phosphorylation by Lck was greatly reduced to 4% of wildtype (Figure S5). Collectively these results indicate that multiple Draper tyrosines are phosphorylated by Src family kinases, and that phosphorylation of non-ITAM residues strongly depends upon ITAM phosphorylation. A potential mechanism for sequential phosphorylation is described in the Discussion.

Discussion

In this study, we have reconstituted Draper-dependent engulfment of PS-coated beads in Drosophila S2 cells and used this system, in conjunction with a liposome-based biochemical assay, to elucidate the initial steps of the phagocytic signaling pathway. Our data reveal that corpse clearance, a conserved process required to recognize and remove dying cells, bears striking mechanistic similarity to mammalian adaptive immune systems, which defend against non-self pathogens and cancer.

Figure 6 shows our working model for Draper triggering. We show that ligation to the lipid PS is sufficient to promote Draper clustering and segregation away from a transmembrane phosphatase (1). Spatial separation between ligated Draper clusters and transmembrane phosphatases shifts a kinase-phosphatase balance in favor of receptor phosphorylation by Src42a, Draper's cognate activating kinase (2). Receptor phosphorylation occurs in a hierarchical manner: Draper's ITAM residues are required for full activation of the system, possibly though direct recruitment of Src42a to Draper's ITAM via its own SH2 domain (2). Phosphorylation of Draper's tail activates a downstream cytosolic signaling cascade, including recruitment of effectors including Shark kinase (3). Receptor phosphorylation and adapter recruitment result in activation of the actin cytoskeleton and the coupling of receptors to actin retrograde flow (4). We note that others have described further downstream Draper signaling outputs, including a positive feedback mechanism to increase expression levels of the receptor itself (*drpr*) (Ziegenfuss et al., 2012) and upregulation of other factors, including matrix metallopeptidase 1 (*mmp1*) (Purice et al., 2017) (4).

PS is an activating ligand for Draper

Draper is reported to recognize both PS (Tung et al., 2013) and the protein ligands Pretaporter and DmCaBP1 (Kuraishi et al., 2009; Okada et al., 2012). For PS, Tung et al (2013) demonstrated direct binding of PS to the extracellular domain of Draper. They also showed that incubation of S2 cells with PS liposomes increased tyrosine phosphorylation levels on Draper, but did not demonstrate a capability of engulfing liposomes. Here we extend this finding to demonstrate that Draper over-expression and ligation to PS are necessary and sufficient to promote efficient engulfment of beads coated with supported lipid bilayers (Fig. 1B). Furthermore, PS is an activating ligand that triggers Draper clustering, localized tyrosine phosphorylation, effector recruitment to mobile microclusters, and remodeling of the actin cytoskeleton. These results provide strong evidence for direct binding of PS to Draper leading to activation of a signaling pathway. The nature of the binding interaction is Our results do not rule out a role for the protein ligands Pretaporter and DmCaBP1 that have been reported previously to act as Draper ligands (Kuraishi et al., 2009; Okada et al., 2012). These additional ligands may allow Draper to respond independently of PS in some contexts.

Mechanism of Draper triggering upon ligation

TCR and FcR activation are driven entirely by phosphorylation of ITAM tyrosines. Shark kinase, like ZAP70, binds specifically to the ITAM motif, and we show that ITAM phosphorylation plays an important role in signaling. However, unlike the TCR, Draper contains non-ITAM tyrosines, and our kinetic assay for phagocytosis shows that non-ITAM tyrosines play a role in the full activation of Draper. Our results are consistent with reports that both ITAM and non-ITAM residues on Draper contribute to signaling (Fujita et al., 2012; Ziegenfuss et al., 2008). The phosphorylated non-ITAM tyrosines in Draper may bind additional SH2-containing adapter proteins- further studies will be needed to identify additional direct binding partners of the phosphorylated cytoplasmic tail domain of Draper besides Shark.

Our in vitro results with a completely biochemically defined system also reveal that Draper's ITAM domain is required for the phosphorylation of the non-ITAM tyrosines. This result indicates a sequential mechanism for multisite phosphorylation on Draper. One model for how this might occur is through the direct recruitment of Src family kinases to the phosphorylated ITAM domain of Draper. The kinase (e.g. Src42a) has a higher specificity for the tyrosines in Draper's ITAM, domain and phosphorylates these residues first. Once phosphorylated, Src42a then can bind to the phosphorylated ITAM through its own SH2 domain; while bound to Draper, the kinase can phosphorylate non-ITAM residues on Draper. A mechanism in which a kinase creates its own binding site before modifying other residues has been suggested for both Src-dependent phosphorylation of synthetic ITAM-containing substrate peptides (Pellicena et al., 1998) and phosphorylation of $p130^{CAS}$ by Abl kinase (Mayer et al., 1995). A similar phenomenon was observed for Lck-dependent modification of sequential ITAM residues on the T cell receptor, which is required for full activation of this receptor (Lewis et al., 1997). Thus, in common with other signaling systems, Draper phosphorylation involves a hierarchal phosphorylation of tyrosines in its tail domain and this hierarchal phosphorylation is required for full receptor activation.

Our findings also may shed light on mechanism of action for phagocytic receptors in organisms beyond the fly. Mammalian glial cells encode a Draper ortholog Megf10, a predicted single pass transmembrane protein with putative ITAMs that recruit Syk kinase (Scheib et al., 2012). Though mechanistic differences likely exist between Draper and Megf10 as a consequence of evolutionary divergence and distinct organismal requirements, Megf10's cytoplasmic tail contains 12 cytoplasmic tyrosine residues, only 4 of which comprise the putative ITAMs (Scheib et al., 2012). Therefore, it will be interesting to investigate if full activation of Megf10 may proceed through a similar sequential, multisite tyrosine phosphorylation mechanism as Draper.

Comparison between Draper triggering and activation of mammalian immune receptors

A potential similarity between Draper and T cell signaling was first suggested by the finding of an ITAM in the Draper cytoplasmic tail (Ziegenfuss et al., 2008). Our findings provide mechanistic support of this idea. T cells are triggered via a kinetic segregation mechanism governed by local shifting of a kinase-phosphatase equilibrium toward receptor phosphorylation (Davis and van der Merwe, 2006). Briefly, apposition of a membrane-membrane interface at the synapse between T cell and the antigen presenting cell (APC) results in the exclusion of the bulky transmembrane phosphatase CD45. When local CD45 concentration is reduced below a threshold, activity of the membrane-bound kinase Lck is favored. Lck phosphorylates the TCR cytoplasmic ITAM motifs which in turn recruit ZAP70 kinase, an essential downstream kinase involved in T cell activation (James and Vale, 2012). A similar segregation mechanism was recently proposed to regulate FcR activation through creating an integrin-based diffusion barrier that excludes CD45 (S. A. Freeman et al., 2016).

Here, we provide evidence that Draper may be activated through a kinetic segregation mechanism. Draper ligation to PS results in the formation of microclusters that are transported by the actin cytoskeleton. The behavior of these microclusters is very similar to that described for the T cell receptor (Bunnell et al., 2002; Douglass and Vale, 2005; Varma et al., 2006). Draper ligation to PS on a second membrane (either an apoptotic cells or an artificial membrane composed of a supported lipid bilayer) also excludes a transmembrane phosphatase from the synapse at the region of receptor phosphorylation and kinase recruitment (Fig. 3A). In the case of T cells, a single transmembrane phosphatase (CD45) is highly expressed on the surface and appears to be the dominant phosphatase in regulating signaling. However, phagocytic cells likely express several transmembrane phosphatases, which together may contribute to

regulating Draper and other phagocytic receptors. Draper is also regulated by at least one cytosolic phosphatase, Corkscrew (Csw, SHP1/2), that is recruited to an alternative short splice isoform of Draper, Draper-II (Logan et al., 2012), that encodes an Immunoreceptor Tyrosine-based Inhibitory Motif (ITIM). In the future, it will be important to determine how the specific composition of phosphatases on the membrane (different sizes and expression levels) are used to dampen and fine-tune the sensitivity of engulfment.

Synthetic engulfment receptors

Analogous to TCRs, the extracellular ligand and receptor for Draper can be functionally replaced by other interacting modules such as FKBP-rapamycin-FRB. These chimeric receptors create signaling zones for both Draper (Fig. 3E) and TCR (James and Vale, 2012). The ability to replace the extracellular modules implies that Draper signaling does not require a ligand-induced conformational change to the cytoplasmic tail, although the possibility that such changes augment signaling cannot be excluded. Our ability to replace Draper and PS with a synthetic FKBP-rapamycin-FRB module also provides a mechanistic basis to reprogram engulfment signaling toward non-native targets. This idea is a conceptually similar to that of chimeric T cell receptors that recognize cancer antigen to promote specific cell killing (Lim and June, 2017). Collectively, we have revealed that understanding the fundamental cell biology and biochemistry underlying early steps of Draper activation provide a mechanistic basis to reprogram engulfment signaling.

Acknowledgements

We thank C. Carbone, E. Hui, N.Kern, M. Morrissey, X. Su, and M. Taylor for reagents and discussions, N. Stuurman for help with microscopy, and L. Kohlstaedt and Y-S Kim (QB3/UC Berkeley) for performing the mass spectrometry. We also thank E. Hui, A. Jain, M. Morrissey, K. McKinley, X. Su, and P. Williamson for critical reading of the manuscript. A.P.W. was supported by a CRI-Irvington Postdoctoral Fellowship. This work was funded by the Howard Hughes Medical Institute and the National Institutes of Health (R01EB007187, R.D.V.).

Author Contributions

A.P.W. and R.D.V. conceived of the study and designed the experiments. A.P.W. performed the experiments, analyzed the data, and prepared the figures. A.P.W. and R.D.V. wrote the manuscript.

Competing Financial Interests

The authors declare no competing financial interests.

References

Arandjelovic, S., Ravichandran, K.S., 2015. Phagocytosis of apoptotic cells in homeostasis. Nat. Immunol. 16, 907–917. doi:10.1038/ni.3253

Bunnell, S.C., Hong, D.I., Kardon, J.R., Yamazaki, T., McGlade, C.J., Barr, V.A., Samelson, L.E., 2002. T cell receptor ligation induces the formation of dynamically regulated signaling assemblies. J. Cell Biol. 158, 1263–1275. doi:10.1083/jcb.200203043

Burroughs, N.J., Lazic, Z., van der Merwe, P.A., 2006. Ligand detection and discrimination by spatial relocalization: A kinase-phosphatase segregation model of TCR activation. Biophys. J. 91, 1619–1629. doi:10.1529/biophysj.105.080044

Cherbas, L., Willingham, A., Zhang, D., Yang, L., Zou, Y., Eads, B.D., Carlson, J.W., Landolin, J.M., Kapranov, P., Dumais, J., Samsonova, A., Choi, J.-H., Roberts, J., Davis, C.A., Tang, H., van Baren, M.J., Ghosh, S., Dobin, A., Bell, K., Lin, W., Langton, L., Duff, M.O., Tenney, A.E., Zaleski, C., Brent, M.R., Hoskins, R.A., Kaufman, T.C., Andrews, J., Graveley, B.R., Perrimon, N., Celniker, S.E., Gingeras, T.R., Cherbas, P., 2011. The transcriptional diversity of 25 Drosophila cell lines. Genome Res. 21, 301–314. doi:10.1101/gr.112961.110

Choudhuri, K., Dustin, M.L., 2010. Signaling microdomains in T cells. FEBS Lett. 584, 4823–4831. doi:10.1016/j.febslet.2010.10.015

Choudhuri, K., Wiseman, D., Brown, M.H., Gould, K., van der Merwe, P.A., 2005. T-cell receptor triggering is critically dependent on the dimensions of its peptide-MHC ligand. Nature 436, 578–582. doi:10.1038/nature03843

Davis, S.J., van der Merwe, P.A., 2006. The kinetic-segregation model: TCR triggering and beyond. Nat. Immunol. 7, 803–809. doi:10.1038/ni1369

Douglass, A.D., Vale, R.D., 2005. Single-molecule microscopy reveals plasma membrane microdomains created by protein-protein networks that exclude or trap signaling molecules in T cells. Cell 121, 937–950. doi:10.1016/j.cell.2005.04.009

Edelstein, A., Amodaj, N., Hoover, K., Vale, R., Stuurman, N., 2010. Computer control of microscopes using μManager. Curr Protoc Mol Biol Chapter 14, Unit14.20–14.20.17. doi:10.1002/0471142727.mb1420s92

Elliott, M.R., Ravichandran, K.S., 2010. Clearance of apoptotic cells: implications in health and disease. J. Cell Biol. 189, 1059–1070. doi:10.1083/jcb.201004096

Etchegaray, J.I., Timmons, A.K., Klein, A.P., Pritchett, T.L., Welch, E., Meehan, T.L., Li, C., McCall, K., 2012. Draper acts through the JNK pathway to control synchronous engulfment of dying germline cells by follicular epithelial cells. Development 139, 4029–4039. doi:10.1242/dev.082776

Evans, I.R., Rodrigues, F.S.L.M., Armitage, E.L., Wood, W., 2015. Draper/CED-1 mediates an ancient damage response to control inflammatory blood cell migration in vivo. Curr. Biol. 25, 1606–1612. doi:10.1016/j.cub.2015.04.037

Fadok, V.A., Voelker, D.R., Campbell, P.A., Cohen, J.J., Bratton, D.L., Henson, P.M., 1992.

Exposure of phosphatidylserine on the surface of apoptotic lymphocytes triggers specific recognition and removal by macrophages. J. Immunol. 148, 2207–2216.

Freeman, M.R., Delrow, J., Kim, J., Johnson, E., Doe, C.Q., 2003. Unwrapping glial biology: Gcm target genes regulating glial development, diversification, and function. Neuron 38, 567–580.

Freeman, S.A., Goyette, J., Furuya, W., Woods, E.C., Bertozzi, C.R., Bergmeier, W., Hinz, B., van der Merwe, P.A., Das, R., Grinstein, S., 2016. Integrins Form an Expanding Diffusional Barrier that Coordinates Phagocytosis. Cell 164, 128–140. doi:10.1016/j.cell.2015.11.048

Freeman, S.A., Grinstein, S., 2014. Phagocytosis: receptors, signal integration, and the cytoskeleton. Immunol. Rev. 262, 193–215. doi:10.1111/imr.12212

Fujita, Y., Nagaosa, K., Shiratsuchi, A., Nakanishi, Y., 2012. Role of NPxY motif in Draper-mediated apoptotic cell clearance in Drosophila. Drug Discov Ther 6, 291–297.

Hui, E., Vale, R.D., 2014. In vitro membrane reconstitution of the T-cell receptor proximal signaling network. Nat. Struct. Mol. Biol. 21, 133–142. doi:10.1038/nsmb.2762

Iram, T., Ramirez-Ortiz, Z., Byrne, M.H., Coleman, U.A., Kingery, N.D., Means, T.K., Frenkel, D., Khoury, El, J., 2016. Megf10 Is a Receptor for C1Q That Mediates Clearance of Apoptotic Cells by Astrocytes. J. Neurosci. 36, 5185–5192. doi:10.1523/JNEUROSCI.3850-15.2016

James, J.R., Vale, R.D., 2012. Biophysical mechanism of T-cell receptor triggering in a reconstituted system. Nature 487, 64–69. doi:10.1038/nature11220

Kaizuka, Y., Douglass, A.D., Varma, R., Dustin, M.L., Vale, R.D., 2007. Mechanisms for segregating T cell receptor and adhesion molecules during immunological synapse formation in Jurkat T cells. Proc. Natl. Acad. Sci. U.S.A. 104, 20296–20301. doi:10.1073/pnas.0710258105

Kuraishi, T., Nakagawa, Y., Nagaosa, K., Hashimoto, Y., Ishimoto, T., Moki, T., Fujita, Y., Nakayama, H., Dohmae, N., Shiratsuchi, A., Yamamoto, N., Ueda, K., Yamaguchi, M., Awasaki, T., Nakanishi, Y., 2009. Pretaporter, a Drosophila protein serving as a ligand for Draper in the phagocytosis of apoptotic cells. EMBO J. 28, 3868–3878. doi:10.1038/emboj.2009.343

Leventis, P.A., Grinstein, S., 2010. The distribution and function of phosphatidylserine in cellular membranes. Annu Rev Biophys 39, 407–427. doi:10.1146/annurev.biophys.093008.131234

Lewis, L.A., Chung, C.D., Chen, J., Parnes, J.R., Moran, M., Patel, V.P., Miceli, M.C., 1997. The Lck SH2 phosphotyrosine binding site is critical for efficient TCR-induced processive tyrosine phosphorylation of the zeta-chain and IL-2 production. J. Immunol. 159, 2292–2300.

Lim, W.A., June, C.H., 2017. The Principles of Engineering Immune Cells to Treat Cancer. Cell 168, 724–740. doi:10.1016/j.cell.2017.01.016

Logan, M.A., Hackett, R., Doherty, J., Sheehan, A., Speese, S.D., Freeman, M.R., 2012.

Negative regulation of glial engulfment activity by Draper terminates glial responses to axon injury. Nat. Neurosci. 15, 722–730. doi:10.1038/nn.3066

Lu, T.-Y., Doherty, J., Freeman, M.R., 2014. DRK/DOS/SOS converge with Crk/Mbc/dCed-12 to activate Rac1 during glial engulfment of axonal debris. Proc. Natl. Acad. Sci. U.S.A. 111, 12544–12549. doi:10.1073/pnas.1403450111

MacDonald, J.M., Beach, M.G., Porpiglia, E., Sheehan, A.E., Watts, R.J., Freeman, M.R., 2006. The Drosophila cell corpse engulfment receptor Draper mediates glial clearance of severed axons. Neuron 50, 869–881. doi:10.1016/j.neuron.2006.04.028

Mayer, B.J., Hirai, H., Sakai, R., 1995. Evidence that SH2 domains promote processive phosphorylation by protein-tyrosine kinases. Curr. Biol. 5, 296–305.

Murugesan, S., Hong, J., Yi, J., Li, D., Beach, J.R., Shao, L., Meinhardt, J., Madison, G., Wu, X., Betzig, E., Hammer, J.A., 2016. Formin-generated actomyosin arcs propel T cell receptor microcluster movement at the immune synapse. J. Cell Biol. 215, 383–399. doi:10.1083/jcb.201603080

Neumann, B., Coakley, S., Giordano-Santini, R., Linton, C., Lee, E.S., Nakagawa, A., Xue, D., Hilliard, M.A., 2015. EFF-1-mediated regenerative axonal fusion requires components of the apoptotic pathway. Nature 517, 219–222. doi:10.1038/nature14102

Okada, R., Nagaosa, K., Kuraishi, T., Nakayama, H., Yamamoto, N., Nakagawa, Y., Dohmae, N., Shiratsuchi, A., Nakanishi, Y., 2012. Apoptosis-dependent externalization and involvement in apoptotic cell clearance of DmCaBP1, an endoplasmic reticulum protein of Drosophila. J. Biol. Chem. 287, 3138–3146. doi:10.1074/jbc.M111.277921

Pellicena, P., Stowell, K.R., Miller, W.T., 1998. Enhanced phosphorylation of Src family kinase substrates containing SH2 domain binding sites. Journal of Biological Chemistry 273, 15325–15328.

Penberthy, K.K., Ravichandran, K.S., 2016. Apoptotic cell recognition receptors and scavenger receptors. Immunol. Rev. 269, 44–59. doi:10.1111/imr.12376

Purice, M.D., Ray, A., Münzel, E.J., Pope, B.J., Park, D.J., Speese, S.D., Logan, M.A., 2017. A novel Drosophila injury model reveals severed axons are cleared through a Draper/MMP-1 signaling cascade. Elife 6, R55. doi:10.7554/eLife.23611

Ravichandran, K.S., Lorenz, U., 2007. Engulfment of apoptotic cells: signals for a good meal. Nat. Rev. Immunol. 7, 964–974. doi:10.1038/nri2214

Reddien, P.W., Horvitz, H.R., 2004. The engulfment process of programmed cell death in caenorhabditis elegans. Annu. Rev. Cell Dev. Biol. 20, 193–221. doi:10.1146/annurev.cellbio.20.022003.114619

Scheib, J.L., Sullivan, C.S., Carter, B.D., 2012. Jedi-1 and MEGF10 signal engulfment of apoptotic neurons through the tyrosine kinase Syk. J. Neurosci. 32, 13022–13031. doi:10.1523/JNEUROSCI.6350-11.2012

Schneider, I., 1972. Cell lines derived from late embryonic stages of Drosophila melanogaster. J

Embryol Exp Morphol 27, 353–365.

Schultz, J., Copley, R.R., Doerks, T., Ponting, C.P., Bork, P., 2000. SMART: a web-based tool for the study of genetically mobile domains. Nucleic Acids Res. 28, 231–234.

Tung, T.T., Nagaosa, K., Fujita, Y., Kita, A., Mori, H., Okada, R., Nonaka, S., Nakanishi, Y., 2013. Phosphatidylserine recognition and induction of apoptotic cell clearance by Drosophila engulfment receptor Draper. J. Biochem. 153, 483–491. doi:10.1093/jb/mvt014

Varma, R., Campi, G., Yokosuka, T., Saito, T., Dustin, M.L., 2006. T cell receptor-proximal signals are sustained in peripheral microclusters and terminated in the central supramolecular activation cluster. Immunity 25, 117–127. doi:10.1016/j.immuni.2006.04.010

Zhou, Z., Hartwieg, E., Horvitz, H.R., 2001. CED-1 is a transmembrane receptor that mediates cell corpse engulfment in C. elegans. Cell 104, 43–56.

Ziegenfuss, J.S., Biswas, R., Avery, M.A., Hong, K., Sheehan, A.E., Yeung, Y.-G., Stanley, E.R., Freeman, M.R., 2008. Draper-dependent glial phagocytic activity is mediated by Src and Syk family kinase signalling. Nature 453, 935–939. doi:10.1038/nature06901

Ziegenfuss, J.S., Doherty, J., Freeman, M.R., 2012. Distinct molecular pathways mediate glial activation and engulfment of axonal debris after axotomy. Nat. Neurosci. 15, 979–987. doi:10.1038/nn.3135

Figure Legends

Figure 1: Cellular reconstitution of Draper signaling

A. Schematic of apoptotic cell clearance by professional phagocytes; multiple receptors including Draper (green) recognize distinct ligands to promote engulfment of dying cell corpses (purple). Representative image of an Annexin V-APC labeled cell corpse fully internalized by a Draper-GFP expressing S2 cell. Overexpression of Draper-GFP in S2 cells results in a ~5 fold increase in phagocytic proficiency toward apoptotic cell corpses. Draper-GFP+ S2 cells were incubated with labeled cell corpses and phagocytic proficiency was assessed after 45 min incubation at 27° C. Results from 3 independent biological replicates are shown (mean ± SD). **B.** Schematic of reconstitution system to study Draper signaling. The cell corpse was replaced with a silica bead coated with a supported lipid bilayer containing phosphatidylserine (PS). Representative image of an atto390-labeled 10% PS bead fully internalized by a Draper-GFP expressing S2 cell. Draper overexpression increases PS-bead phagocytic proficiency ~7 fold. S2 cells were transfected with either Draper-GFP or a GFP control vector and incubated with PC or 10% PS beads for 30 min at 27° C. The mean number of beads fully ingested per cell for three independent biological replicates are shown (mean ± SD). **C.** Draper-GFP expressing S2 cells were incubated with beads containing increasing mol. % of PS in the supported lipid bilayer and phagocytic proficiency was assessed after 30 min incubation at 27° C (mean ± SD). **D.** Upon completion of the phagocytic cup, beads internalized. Draper-GFP/Lifeact-BFP S2 cells were incubated with 10% PS/0.1% rhodamine-PE beads and imaged every 3 min by spinning disk confocal microscopy. A middle section from a z-stack movie is shown. Stills are taken from Movie 1. Upon completion of the phagocytic cup (as assessed by Lifeact), internalization of the bead occurs. Scale bars, 5 μm.

Figure 2: Draper organizes into mobile microclusters that recruit signaling molecules

A. Draper-GFP is tyrosine phosphorylated at the interface with a 10% PS bead. Draper-GFP+ S2 cells were incubated with 10% PS beads. After 30 min incubation cells were fixed, permeabilized and stained with phosphotyrosine (pTyr) antibody. pTyr staining is enriched at the synapse between bead and cell. During fixation and permeabilization, the supported lipid bilayer on the bead is stripped off; bead position is indicated by dashed white line. **B.** Shark kinase is enriched at the synapse between 10% PS bead and the S2 cell. S2 cells were co-transfected with Draper-GFP and Shark-mCherry and incubated with 10% PS beads labeled with 0.5% atto390-DOPE. After 15 min, cells with active synapses were imaged by spinning disk confocal microscopy. The middle slice from a z-stack is shown. **C.** Schematic of TIRF-M assay setup to visualize ligated Draper-GFP at the plasma membrane. Draper-GFP+ S2 cells were allowed to settle on 10% PS supported lipid bilayer (SLB) prepared on a glass coverslip, and Draper-GFP+ was imaged directly in real time. **D.** Draper-GFP forms microclusters on 10% PS SLB. Draper-GFP microclusters visualized by TIRF-M undergo retrograde flow towards a central synapse. Microclusters fuse with one-another and are repopulated from the periphery. Time in min:sec. **E.** Draper-GFP microclusters on 10% PS bilayers recruit Shark-TagBFP and Crk-mCherry to the plasma membrane. Cells co-transfected with receptor, kinase and adapter were allowed to settle on 10% PS bilayers as D. and imaged after spreading. Scale bars, 5 μm.

Figure 3: Segregation of Draper and a transmembrane phosphatase at the synapse

A. The transmembrane phosphatase Ptp69D segregates away from Draper at synapses between 10% PS beads and the S2 cell. Draper-mCherry and Ptp69D-GFP were co-transfected into S2 cells and localization at the synapse after a 15 min incubation. **B.** Schematic showing extracellular FRB fused to the Draper transmembrane and cytosolic domains (FRB-EXT-Draper-INT) to program clearance signaling towards FKBP-bearing beads (see Methods). FRB and FKBP are brought together into a 100 fM ternary complex in the presence of 1 μM rapamycin. **C.** FRB-EXT-Draper-INT promotes specific phagocytosis of FKBP beads. S2 cells transfected

with FRB-EXT-Draper-INT were incubated with 10 nM FKBP beads for 30 min, after which bead ingestion was quantified after imaging using spinning disk confocal microscopy (see Methods). The mean number of beads fully ingested per cell for three independent biological replicates are shown (mean ± SD). Cells were incubated either with 1 μM rapamycin (right, +) or an equivalent volume of DMSO vehicle (left, -). **D.** The kinase Shark is recruited to FRB-EXT-Draper-INT, indicating local receptor activation by tyrosine phosphorylation. S2 cells expressing FRB-EXT-Draper-INT-GFP and Shark-Cherry were incubated with FKBP beads coupled to 10 nM his10 protein (see Methods) in the presence of 1 μM rapamycin for 15 min and localization was assessed. A middle section from a confocal z-stack is shown. **E.** S2 cells were transfected with FRB-EXT-Draper-INT-mCherry, Shark-TagBFP, and Ptp69D-GFP and allowed to settle on SLB with bound His_{10}-FKBP bilayers in the presence of 1 μM rapamycin for 15 min. Ptp69D segregates away from activated Draper at the interface between FKBP bilayer and S2 cell. In contrast, Draper and Shark overlapped, indicating local receptor activation and segregation away from Ptp69D at the synapse. Scale bars, 5 μm.

Figure 4: Roles of Draper's cytoplasmic tyrosine residues in engulfment of PS beads

A. Engulfment of 10% PS beads by S2 cells expressing Draper-GFP, Draper-Ala11-GFP, or a GFP control was assessed after 45 min incubation. Mean number of beads ingested per cell for three biological replicates are shown (mean ± SD). **B.** Alignment of residues mutated to Phe in Draper-ΔITAM. **C.** Draper-ΔITAM displays a kinetic delay and reduced phagocytic proficiency relative to Draper-GFP, while Draper's ITAM (ITAM only) is sufficient for partial engulfment activity. S2 cells transfected with Draper-GFP or indicated mutants were incubated with 10% PS beads, allowed to settle, and imaged at the indicated time points. The mean number of beads fully ingested per cell for three independent biological replicates are shown (mean ± SD).

Figure 5: In vitro reconstitution of hierarchical multisite Tyr phosphorylation on Draper

A. Schematic of liposome-FRET assay to detect direct binding between Draper's phosphorylated tail and SH2-domain containing reporter proteins. Assay is described in detail in the Methods. Briefly, when a BG505-labeled reporter protein comes into close proximity to a rhodamine labeled liposome, the 505 nm fluorescence signal is quenched. If quenching that occurs after addition of ATP binding is likely due to the Src42a-dependent phosphorylation of Draper's cytoplasmic tyrosine residues. The results shown here reveal that direct binding of BG505-Shark-tSH2 to Draper's tail is dependent on an intact ITAM on Draper. His_{10}-Draper cytosolic domain or His_{10}-DraperY934F/Y949F (ΔITAM) receptor tail were ligated to 0.5% rhodamine-PE liposomes and ATP dependent quenching was assessed.

B. On-liposome phosphorylation reactions to assess Draper activation by its cognate Src family kinase Src42a. His_{10}-Draper cytoplasmic domain or 10his-DraperY934F/Y949F (ΔITAM) receptor tail (both at 1 μM) were ligated to liposomes doped with DGS-Ni-NTA and incubated with 86 nM soluble Src42a and 1 mM ATP for 30 min. Reactions were quenched with SDS-PAGE buffer containing DTT and 2-Me and boiled for 10 min at 95°C. Samples were immunoblotted with phosphotyrosine antibody or His_{10} antibody. Quantification of phosphorylation of WT or ΔITAM by Src42a was determined as the ratio of total pTyr signal very total His_{10} signal internally for each lane. **C.** On-liposome phosphorylation reactions to assess Draper activation by Src42a (86 nM) were performed as above. 1 μM His_{10}-Draper cytoplasmic domain were phosphorylated as 5B above with the exception that samples were quenched using 10 mM EDTA and 8 M Urea and digested for 1D mass spectrometry (see Methods)**.** Height of bar corresponds to percent phosphorylated peptide (number of phosphorylated peptides detected divided by total number of peptides detected). Total peptides detected for each site residue in parentheses: Y838 (14), Y858 (14), Y888 (9), Y901 (29), Y905 (29), Y924 (71), Y934 (68), Y943 (7), Y949 (10), Y954 (10), Y965 (0).

Figure 6: Mechanism of Draper triggering

(1) Draper ligation to PS on a cell corpse creates an exclusion zone where ligated receptors cluster at the synapse and unligated molecules such as bulky transmembrane phosphatases segregate away from receptors. (2) Spatial segregation between receptors and inhibitory phosphatases shifts the balance towards receptor phosphorylation by Src42a, a reaction strikingly similar to triggering of TCRs by the kinase Lck. Src42a first phosphorylates Draper's ITAM and then modifies non-ITAM Tyr residues that also contribute to signaling. (3) Tyr phosphorylation on Draper's tail recruits cytosolic effector proteins including the kinase Shark in a manner similar to recruitment of the kinase ZAP70 to triggered TCRs. (4) Effector recruitment to phosphorylated Draper molecules promotes signaling outputs including cytoskeletal remodeling and engulfment.

Movie Legends

Movie 1: Cellular reconstitution of Draper signaling

Movie of stills shown in Fig. 1D. An S2 cell co-transfected with Draper-GFP and Lifeact-BFP was incubated with 10% PS/0.5% atto647-PE 6.4 μm silica beads. Movie is a maximum projection of a z-stack (1 μm between z-positions). Z-stacks captured by spinning disk confocal microscopy were recorded every 3 min. Scale bar, 5 μm.

Movie 2: Formation of mobile Draper-GFP microclusters on 10% PS bilayers

Movie of stills shown in Fig. 2D. An S2 cell transfected with Draper-GFP was allowed to settle on 10% PS supported lipid bilayers and imaged by TIRF microscopy. Cell was imaged every 15 sec. Draper-GFP forms mobile microclusters that appear at the edge of the spread cell and migrate toward the prominent central synapse. Scale bar, 5 μm.

Movie 3: Visualization of Draper and F-actin on 10% PS bilayers

An S2 cell co-transfected with Draper-mCherry and Lifeact-eGFP was allowed to settle on 10% PS supported lipid bilayers and imaged by TIRF microscopy. Cell was imaged every min. Channels were split so Draper-mCherry and Lifeact-eGFP can be visualized simultaneously. Note the F-actin “hole” visible at the last timepoint, where the central synapse of Draper-mCherry signal appears to exclude F-actin as visualized by Lifeact-eGFP. Scale bar, 5 μm.

Movie 4: Visualization of signaling microclusters on 10% PS bilayers

Movie of stills shown in Fig. 2E. An S2 cell co-transfected with Draper-GFP, Shark-TagBFP, and Crk-mCherry was allowed to settle on 10% PS supported lipid bilayers and imaged by TIRF microscopy. Cell was imaged every 15 sec. Draper-GFP, Shark-TagBFP, and Crk-mCherry co-localize at mobile microclusters that flow towards the central synapse. Scale bar, 5 μm.

Movie 5: Visualization of FKBP-Bead engulfment by a chimeric FRB-Draper receptor

An S2 cell, co-transfected with FRB-EXT-Draper-INT-mCherry and Lifeact-eGFP, was incubated with 2% DGS-Ni-NTA/0.5% atto390-PE 6.46 μm silica beads incubated with 10 nM His_{10}-FKBP, washed, and resuspended prior to imaging. FKBP beads were incubated with co-transfected S2 cells in the presence of 1 μM rapamycin, allowed to settle in the imaging chamber for 5 min, and visualized at 5 min intervals by spinning disk confocal microscopy. Scale bar, 5 μm.

Supplementary Figure Legends

Figure S1 (related to Figure 2): p85 and Crk are recruited to Draper rich synapses with 10% PS beads

Draper-mCherry's ability to bring the indicated SH2-GFP proteins to the plasma membrane at the synapse with a 10% PS bead. Shark, p85 (the PI3K activating subunit), and Crk were recruited to Draper-mCherry at the synapse,while Stat92E was not recruited. Scale bars indicate 5 μm.

Figure S2 (related to Figure 3): The transmembrane phosphatase Ptp69D.

A. Drosophila S2 cells express an array of transmembrane phosphatases. RNA levels measure by RNA-Seq (NLM/NCBI GEO GSM410195), organized in descending order of RNA measured, indicated in reads per kilobase of exon model per million mapped reads (RPKM). **B.** Schematic of Ptp69D-GFP domain structure, highlighting features of its bulky extracellular domain. **C.** Draper-mCherry clusters exclude Ptp69D-GFP on 10% PS supported lipid bilayers (SLBs). Draper-mCherry/Ptp69D-GFP expressing S2 cells were allowed to settle and spread on bilayers and localization of receptor and phosphatase assessed after 15 minutes. Phosphatase exclusion was observed both at peripheral clusters and the central synapse. Scale bar indicates 5 μm.

Figure S3 (related to Figure 4): Draper's ITAM is necessary and sufficient to recruit Shark in cells.

S2 cells co-transfected with Draper, Draper-ΔITAM, or Draper- ITAM Only-GFP and Shark-TagBFP were incubated with 10% PS beads labeled with 0.5% atto647-PE. Localization of receptor and Shark-TagBFP was assessed after 15 min cell settling by spinning disk confocal

microscopy. Images were acquired using the same microscope settings and scaled equally for comparison. Scale bars indicate 5 μm.

Figure S4 (related to Figure 5): Identification of phosphorylation sites on Draper by Lck

A. On-liposome phosphorylation reactions to assess Draper activation by His10-Lck-Y505F (1 nM) was performed as Fig. 5. 1 μM His10-Draper cytoplasmic domain was phosphorylated andquenched using 10 mM EDTA and 8 M Urea and digested for 1D mass spectrometry. Height of bar corresponds to percent phosphorylated peptide divided by total number of peptides detected. Total peptides detected for each site residue in parentheses: Y838 (0), Y858 (0), Y888 (4), Y901 (35), Y905 (35), Y924 (15), Y934 (16), Y943 (0), Y949 (0), Y954 (0), Y965 (0).

B. To perform on-liposome phosphorylation reactions to assess Draper activation by Lck, 1 μM 10his-Draper cytoplasmic domain or 10his-DraperY934F/Y949F (ΔITAM) receptor tail were ligated to liposomes doped with DGS-Ni-NTA and incubated with 1 nM his10-Lck-Y505F and 1 mM ATP for 30 min. Reactions were quenched with SDS-PAGE buffer containing DTT and 2-Me and boiled for 10 min at 95oC. Samples were run on a 4-20% gradient gel and pan phosphotyrosine (800 nm anti-mouse secondary) was assessed by western blotting and Licor imaging. Presence of receptor tail was confirmed using his probe (700 nm anti-rabbit secondary). Quantification of phosphorylation of WT or ΔITAM by Lck was determined as the ratio of total pTyr signal:total his signal internally for each lane and reported as the % signal on ΔITAM.

Methods

Note: See the completed **KEY RESOURCES TABLE** for supplier and catalog information

Contact for Reagent and Resource Sharing

Requests for further information and reagents should be directed to and will be fulfilled by the corresponding author, Ronald D. Vale (ron.vale@ucsf.edu).

Experimental Model and Subject Details

Drosophila S2 Cell Culture

Drosophila S2U cells were cultured in Schneider's media (Gibco) supplemented with 10% Fetal Bovine Serum (FBS, Atlanta) and 1x antibiotic-antimycotic (Gibco). S2 cells were grown in non-vented T25 or T75 flasks (Corning) and split every 3-6 days from high density cultures (~50-80%). S2U cells were not split to below ~25% confluency as S2U cells are unhappy at low density. Healthy S2U cells adhere gently to the surface of the culture dish rather than floating, but can be split by gently resuspending the adhered cells using a tissue culture pipet and a 10 ml sterile tissue culture pipet. Enzymatic dissociation using trypsin or by scraping is unnecessary for S2U cells. Frozen stocks were prepared regularly. S2U freeze media is: 45% fresh complete media, 45% sterile filtered conditioned media prepared after spinning the media for 5 min at 1000 x g, and 10% DMSO (Sigma). A confluent T75 dish of S2U cells was pelleted for 5 min at 1000 x g, resuspended in 10 ml of freeze media (described above) and split as 1 ml aliquots in externally-threaded cryotubes (Corning), stored at -80°C in a cell freezing apparatus

containing isopropyl alcohol, and transferred to long term storage in liquid nitrogen, vapor phase. Cells were regularly tested for mycoplasma using the MycoAlert kit (Lonza).

Method Details

Transfection of Drosophila S2U Cells

Cells were split to ~60% confluency into 6 well tissue culture dishes 4 to 12 hr prior to transfection. All transfection mixes were prepared in 5 ml low-retention polystyrene round-bottom tubes. To prepare transfection mixes a maximum of 2.5 µg plasmid DNA was added to 300 µl serum-free Schneider's media and gently mixed. 5 µl of TransIT-Insect (Mirus) was added to diluted DNA and gently mixed. At this point the solution appears cloudy. Transfection mixes were incubated at room temperature for 15 min and added drop-wise gently to the 6 well plate using a p1000 pipet. After drop-wise addition of transfection mixes, the plate was gently shaken laterally to ensure even distribution of TransIT-DNA particles. Transfection efficiencies of at least 50% and up to 90% were regularly obtained using this method, an improvement compared to other transient transfection methods employed for Drosophila S2U cells.

All constructs used in this study express proteins of interest in S2U cells were under control of a pMT copper-inducible promoter. To induce expression in transfected cells, $CuSO_4$ was added from a 50 mM sterile stock in water to a final concentration of 250 µM (1 to 200 dilution from stock) 36 to 48 hr after transfection. The timing of induction is important – at this later time point, we find expression levels to be lower and more uniform. At shorter time points (e.g. 12 to 24 hr after transfection), transfection efficiency was lower and expression levels in transfected cells higher, as assessed by live cell imaging of fluorescent proteins under control of the pMT promoter.

Preparation of APC Annexin V Labeled Apoptotic Cell Corpses

To prepare labeled apoptotic cell corpses for use in internalization assays, 1 μM final concentration of Actinomycin D (Sigma; 1 mg/ml in DMSO, 833 μM stock) was added directly to 80% confluent cultures of Drosophila S2U cells in 6 well plates. Cells were incubated for 16 hr in Actinomycin D prior to harvesting by centrifugation for 5 min at 1000 x g in a 15 ml falcon tube. Actinomycin D was washed out by rinsing corpses twice in complete Schenider's media in the same falcon tube – sequential washes, each with 10 ml complete media were performed. Corpses from 1 well of a 6 well dish were resuspended in 300 μl of complete media after washes and transferred to a 1.7 ml Eppendorf tube for labeling. To label externalized phosphatidylserine (PS), APC Annexin V (BioLegend) was added directly to the washed corpses to a final concentration of 50 ng/ul (from 5 μg/ml stock). The tube was wrapped in foil prior to labeling on a rotator at room temperature for 30 min. After labeling, cells were washed 3 times by sequential harvesting and resuspension in complete media. After washing labeled corpses were resuspended in 300 μl complete media.

Assay for Internalization of Apoptotic Cell Corpses

To assess internalization of apoptotic cell corpses, washed Draper-GFP or mCherry-control transfected S2U cells were incubated with labeled cell corpses prepared as above. Transfected cells were washed with complete S2U media, and culture media was replaced with 1 ml of fresh. Cells in fresh media were gently resuspended by pipetting up and down. 10 μl of the washed labeled cell corpses prepared as above were mixed in an Eppendorf tube with 300 μl of washed transfected cells. Eppendorf tube was flipped up and down 4 times and complete mixture was plated in 1 well of a 96-well glass bottomed MatriPlate imaging dish (Brooks). After

45 min incubation at room temperature in the dark, High Content Screening imaging and quantification were performed as described below.

Preparation of 10% PS-coated Silica Beads

10 molar % phosphatidylserine (PS) beads were used for all experiments other than the PS titration in Figure 1G. To prepare 10 molar % beads, chloroform suspended lipids sufficient for 1 ml of a 10 mM solution were mixed at the following proportions: 89.5% POPC, 10% DOPS, 0.5% PEG5000-PE, 0.5% atto390-DOPE (label for visualization by microscopy). Lipids were transferred to a chloroform-washed glass vial using gas-tight Hamilton syringes and dried to a film under argon gas in a warm (~45° C) water bath. Dried lipids were stored under foil (if labeled lipids were used) and desiccated overnight at room temperature in a benchtop desiccator filled with Drierite. Dried lipids were suspended in 1 ml tissue culture grade PBS by vortexing for 1 min under parafilm and gentle pipetting. Suspended lipids were transferred to a 1.7 ml Eppendorf tube and stored under argon gas. The PBS-lipid mix was freeze/thawed 5 times in liquid nitrogen/warm water and subjected to 2 x 5 min sonication in a Bioruptor Pico bath sonicator (Diagenode). Sonicated lipids were spin at 35000 rpm for 35 min at 4° C in a TLA 120.1 rotor in a benchtop Beckman ultracentrifuge. Only a small pellet should be visible after spinning sonicated lipids. Small Unilamellar Vesicles (SUVs) prepared using this method were used immediately or stored under argon gas, flash frozen, and stored at -80° C. Lipid mixes are best used within two weeks of preparation. Undiluted 10 mM lipid mixes were used as described below to build bilayers on silica beads. For the PS titration in Figure 1G differences in PS concentration were made up by balanced changes to the molar % of PC such that final lipid concentration in 1 ml PBS matched the 10 mM concentration described above.

50 µl 6.46 µm silica beads (Bangs, Catalog #SS06N) were added to 300 µl Milli-Q water in 1.7 ml Eppendorf tubes for washing. Beads in suspension were pelleted 3 times in 300 µl Milli-Q water at 300 rcf and decanted. After the third wash, beads were resuspended in ~30 µl PBS until the pellet was barely covered. 300 µl of 2 mM final concentration of the desired lipid mix (diluted from 10 mM stock in PBS) was vortexed briefly, wrapped in foil, and rotated at room temperature for 45 min. Beads were pelleted and washed 3 times by sequential pelleting and resuspension in 300 µl fresh PBS. Washed beads were resuspended in 300 µl fresh PBS for bead assay, described below.

Assay for Internalization of PS-coated Silica Beads

To assess internalization of PS-coated silica beads, 7 µl of bead suspension was mixed with 300 µl washed transfected S2U cells, flipped gently to mix 4 times, and the complete mixture plated in 1 well of a 96-well glass bottomed MatriPlate imaging dish (Brooks). Cells were allowed to settle and imaged as described below. For endpoint assays, quantification was performed on images taken 30 or 45 min after plating. For kinetic experiments, imaging was started 5 min after plating. Engulfment experiments were performed using S2U cells co-transfected with GFP or a GFP-fusion receptor protein, mCherry-CAAX (full-length mCherry-LEKMSKDGKKKKKKSKTKCVIM) for visualizing plasma membranes during quantification (described below), and 10% PS atto390-PE labeled silica beads.

Assay for Internalization of his10-FKBP Silica Beads

Engulfment experiments using his10-FKBP ligated beads were performed as above with the exception that FRB-EXT-Draper-INT-GFP expressing S2 cells were co-transfected with mCherry-CAAX to serve as a specific receptor for the FKBP ligand. Silica beads above were

prepared as above with the exception that instead of the 10% PS lipid mix, the following lipid mix was used: 97% POPC, 2% DGS-NTA-Nickel, 0.5% PEG5000-PE, 0.5% atto390-DOPE. Beads were blocked for 15 min in 300 µl PBS + 0.1% w/v BSA. His_{10}-FKBP was diluted to 10 nM final concentration in PBS + 0.1% w/v BSA and 300 µl of this dilution was added to each 50 µl bead pellet, as described above. Proteins were coupled to beads for 40 min under foil on a rotator at room temperature, washed 3 x 5 min in PBS + 0.1% w/v BSA and resuspended in PBS + 0.1% w/v BSA prior to the engulfment assay. 300 µl washed transfected cells were mixed with 7 µl His_{10}-FKBP ligated beads either in the presence of 1 µM rapamycin or a matching volume of DMSO (vehicle), flipped 4 times to mix, and ingestion was quantified as described below.

Staining for Phosphotyrosine (pTyr) and the Synapse between S2 Cell and Bead

To fix and stain bead-cell synapses in chambers described above for phosphotyrosine (pTyr) localization, half the media (~150 µl) from imaging chambers was gently removed and replaced with 150 µl 6.4% paraformaldehyde. Cells were fixed under foil for 15 min, washed 2 x 3 min in PBS, permeabilized with 0.5% v/v Triton X-100 in PBS for 10 min, and set overnight to block in PBS + 0.1% v/v TritonX-100 + 0.2% w/v BSA at 4° C wrapped in parafilm in the dark. Cells were stained in primary antibody (pY-20 mouse anti-phosphotyrosine (Santa Cruz), 2 µg/ml final concentration, 1:100 dilution) for 1 hr at room temperature in the dark, washed 3 x 5 min room temperature in PBS + 0.1% v/v Triton X-100 + 0.2% w/v BSA, and incubated in secondary antibody (Thermo, anti-mouse IgG H+L Alexa Fluor 647 conjugated) for 1 hr at room temperature, washed 3 x 5 minutes in PBS + 0.1% v/v Triton X-100 + 0.2% w/v BSA. Washed fixed stained cells were gently covered in 200 µl PBS prior to imaging. Cells were imaged immediately or stored for up to 2 days at 4° C in the dark, wrapped in parafilm before imaging my spinning disk confocal microscopy (see below).

Building PS-containing Supported Lipid Bilayers (SLBs)

The night before the experiment, a 96 well MatriCal imaging plate was submerged in 2% v/v Hellmanex III, microwaved for 2.5 min on full power, and set on a stir plate under saran wrap for at least 12 hr. Hellmanex was washed away through 20 sequential washes using Milli-Q water and the washed plate dried under Nitrogen gas. The dried plate was covered in thermal paper using a roller. The desired number of wells were exposed using a razor and washed 3 x 5 min 5N NaOH. After NaOH washes, wells were cleaned 10 times with MilliQ water.

To prepare 10% PS bilayers, 250 µl 2 mM lipid mix in PBS described above gently pipetted on the glass surface. The lipid mix was pipetted up and down and bilayer formation was allowed to proceed for 30 min at room temperature. After bilayers formed, washes were performed using PBS 3 x 5 min. For each wash, PBS was gently pipetted up and down over the surface of the bilayer to remove SUVs not part of the SLB. Bilayers were washed into serum free Schneider's media prior to adding cells. Imaging on bilayers should be complete within 45 min for best results, as bilayer integrity cannot be assumed after this time.

After washing the SLB, 150 µl of washed cells were added to the surface, allowed to settle, and imaged by Total Internal Reflection Fluorescence-Microscopy as described below. A lower density of cells can be used, as cells will spread on bilayers and imaging overlapping cells is not ideal.

Building His_{10}-FKBP Bearing Supported Lipid Bilayers (SLBs)

Bilayers were prepared as above with the exception that the following lipid mix was used (note the use of DGS-NTA-Nickel lipid to ligate His_{10} proteins to the bilayer): 97% POPC, 2% DGS-NTA-Nickel, 0.5% PEG5000-PE, 0.5% atto390-DOPE or 0.5% atto647-DOPE for labeling, depending on the fluorescent proteins present on fusion proteins assessed. Washed bilayers were blocked in PBS + 0.1% w/v BSA for 15 min prior to protein coupling. To couple His_{10}-FKBP to 2% DGS-NTA-doped bilayers, His_{10}-FKBP was diluted to 10 nM final concentration in PBS + 0.1% w/v BSA and added to SLBs to couple for 40 min at room temperature. Uncoupled protein was washed 3 x 5 min under foil at room temperature prior to adding cells as above with the exception that when FKBP ligand was used with receptors fused to FRB-extracellular domains, 1 μM rapamycin was added to form the 100 fM FRB-rapamycin-FKBP ternary complex.

Liposome FRET Assay for Effector Recruitment to Phosphorylated Receptor Tails

This assay was based upon one used to reconstitute mammalian T cell signaling (Hui and Vale, 2014). To present receptor tails in physiological geometry for phosphorylation by Src-family kinases, 1 μM His_{10} receptor tails (either His_{10}-Draper-INT or His_{10}-Draper- ΔITAM-INT) were ligated to liposomes comprised of the following molar percent: 74.5% POPC, 10% DGS-NTA, 0.5% Rhodamine-PE, 15% DOPS. Liposomes were prepared using an extruder with 200 nm filters (Avanti). Receptor tails and 1 nM His_{10}-Lck-Y505F or 86 nM Src42a (soluble) were equilibrated with receptor tails in the presence of BG505-kinase-tSH2 reporter proteins were incubated. After proteins were allowed to bind for 40 min at room temperature in the dark. At this point, Mg-ATP was added to a 1 mM final concentration and BG505 signal was assessed at indicated time points. Quenching of BG505 signal, dependent upon addition of ATP, indicates recruitment of reporters to phosphorylated receptor tails. Quenching of the BG505 dye was assessed using a Synergy H4 plate reader (BioTek).

Determining Sites of Tyrosine Phosphorylation by 1D Mass Spectrometry

To determine sites of Tyr phosphorylation on Draper (Figure 6), 1 μM His_{10}-Draper-INT was ligated to unlabeled liposomes: 74.5% POPC, 10% DGS-NTA, 15% DOPS and phosphorylated by 1 nM His_{10}-Lck-Y505F after 40 min of protein coupling to liposomes. 100 μl Reactions were quenched with 100 μl of 8 M Urea and 20 mM EDTA at the indicated time points (final concentrations of 4 M urea and 10 mM EDTA) and shock frozen in liquid nitrogen until all reactions were trypsinized in parallel for analysis by mass spectrometry. To perform trypsinization, reactions were thawed by boiling, supplemented with 5 mM final concentration of TCEP, and incubated for 20 min at room temperature. After denaturation samples 10 mM final concentration of iodoacetamide (IAA) as added. Samples were then incubated in the dark for 15 min. Urea concentration was reduced two-fold through addition of 200 μl PBS. 1 mM final concentration of $CaCl_2$ and 1 μg/ml Trypsin Gold (Promega) was added before samples were incubated overnight in the dark at 37° C. Trypsinzation was quenched through addition of 100 μl 0.1% v/v mass spec grade formic acid. Samples were then subjected to 1D mass spectrometry and peptides containing the characteristic shift for phosphorylation (+79.9663 Da) and quantified as described below.

Immunoblot Analysis

To determine degree of tyrosine phosphorylation on His_{10}-Draper intracellular domains, on liposome phosphorylation assays were performed as above and quenched using SDS-PAGE buffer + DTT and incubated for 5 min at 95°C. Reactions were run on 4-20% gradient SDS-PAGE gels and transferred onto nitrocellulose membranes using the iBlot system (Invitrogen). Membranes were blocked for 1 hr at room temperature in PBS + 0.1% w/v bovine serum albumin (BSA, Sigma) and incubated overnight at 4°C with anti-His probe (rabbit) and anti-

phosphotyrosine (mouse) antibodies (Key Resources Table). Primary antibodies were incubated with membranes simultaneously. Both were used at 1:1000 final dilution PBS + 0.1% w/v BSA. Membranes were washed 3 x 5 minutes at room temperature in PBS + 0.1% w/v BSA and incubated with Licor secondary antibodies at 1:10,000 dilution (700 nm anti-rabbit, 800 nm anti-mouse, Key Resources Table) for 1 hr at room temperature. Membranes were washed 3 x 5 minutes at room temperature in PBS + 0.1% w/v BSA and imaged using a Licor Odyssey gel imager. Quantification of anti-phosphotyrosine and anti-his intensity was performed using the Gel Analysis feature of Fiji.

Protein Expression, Purification, and Labeling

His_{10}-Draper and His_{10}-Draper-ΔITAM were transformed into BL-21 DE3 RIPL cells (Agilent). Cells were grown in Terrific Broth (TB), 12 g tryptone, 24 g yeast extract, 4 ml glycerol up to 1L in MilliQ water + 10% v/v sterile salt solution in MilliQ water: 0.17M KH_2PO_4, 0.72 M K_2HPO_4, until cells reached an OD_{280} of ~0.6-0.8, chilled in a 4°C room, and induced overnight by addition of 0.5 mM final concentration of IPTG. Protein expression was performed in shaker set to 18°C. Bacterial pellets were resuspended in lysis buffer (50 mM HEPES, pH 7.5, 300 mM NaCl, 1 tablet Complete EDTA-free protease inhibitor tablet crushed per 100 ml buffer). Lysates were prepared by probe sonication and bound to Ni-NTA agarose (Qiagen). Beads were washed extensively with lysis buffer and proteins eluted in 500 mM imidazole in lysis buffer. Imidazole elutions were subjected to gel filtration chromatography using a Superdex 200 10/30 column (GE Healthcare) in gel filtration buffer: 50 mM HEPES, pH 7.5, 150 mM NaCl, 10% glycerol, and 1 mM TCEP. Monomer fractions were pooled, shock frozen in liquid nitrogen, and stored in small aliquots at -80°C. Soluble Src42a was purified from SF9 cells as a GST-(PP)-SNAP-Src42a fusion where PP indicates a cut site for Precission Protease. Precission Protease cleavage was performed overnight and post-cleavage supernatants were gel filtered as

described below. His_{10}-Lck Y505F was purified from SF9 cells over Nickel agarose (Qiagen) and eluted in 500 mM imidazole in lysis buffer. Both Src family kinases were subjected to gel filtration chromatography using a Superdex 200 10/30 column (GE Healthcare) in gel filtration buffer: 50 mM HEPES, pH 7.5, 150 mM NaCl, 10% glycerol, and 1 mM TCEP. Monomer fractions were pooled, shock frozen in liquid nitrogen, and stored in small aliquots at -80°C. The tandem SH2 domain reporter for Shark kinase was cloned as a GST-(PP)-SNAP-Shark-tSH2 fusion where PP indicates a cut site for Precission Protease. The soluble SNAP-Shark-tSH2 reporter was generated by on-resin cleavage with Precission Protease during purification. GST-Precission Protease remained on the beads. Cleavage products were subjected to gel filtration chromatography using a Superdex 200 10/30 column (GE Healthcare) in gel filtration buffer: 50 mM HEPES, pH 7.5, 150 mM NaCl, 10% glycerol, and 1 mM TCEP. To prepare BG505-labeled SNAP-Shark-tSH2 for the liposome FRET assay, 10 μM cleaved, gel filtered monomer was incubated at a 1:2 molar ratio with SNAP-Cell 505 Star (NEB) overnight in the dark at 4°C and run over a PD Minitrap G-25 column (GE Healthcare) to eliminate excess dye.

Spinning Disk Confocal Microscopy

All internalization and bead co-localization imaging performed for this study was done of a spinning disk confocal microscope (Nikon Ti-Eclipse inverted microscope with a Yokogawa spinning disk). For bead internalization kinetic assays images were acquired using a 40x/0.95 N/A air objective. Live image acquisition for internalization of corpses and beads was performed using the High Content Screening (HCS) Site Generator plugin in μManager. All other images were acquired using a 100x 1.49 N/A oil immersion objective. Images were captured using an Andor iXon EM-CCD camera. The open source μManager software package was used to run the microscope and capture the images.

Total Internal Reflection Fluorescence-Microscopy (TIRF-M)

All SLB imaging was performed using a TIRF microscope equipped with a motorized TIRF arm and a Hamamatsu Flash 4 camera. For all TIRF-M imaging images were captured at 2 x 2 binning. The open source μManager software package was used to run the microscope and capture the images (Edelstein et al., 2010).

Imaging processing and analysis

All image quantification was done on raw, unprocessed images. All images in figures were opened in ImageJ. A middle z-slice was extracted and the channels split. The image intensities were scaled to enhance contrast in Photoshop (Adobe) using appropriate levels of linear adjustment. Background correction was not performed. Where mutants are compared in the same series, images are acquired using identical microscope and camera settings and scaled to equal intensity values.

Quantification and Statistical Analysis

For both corpse internalization and bead internalization assays, targets were scored as internalized following complete engulfment of the object, as assessed by visible mCherry-CAAX or receptor-GFP signal visible completely around the target in stills from live imaging. Beads or corpses attached but not internalized were not scored. Only targets with labeled Annexin V or atto390 visible were scored as internalized. At least 150 cells per condition are shown. Mean value and ± one standard deviation are plotted (GraphPad 6.0).

Data Availability

Requests for raw data in support of the conclusions of this study should be directed to and will be fulfilled by the corresponding author, Ronald D. Vale (ron.vale@ucsf.edu).

KEY RESOURCES TABLE

REAGENT or RESOURCE	SOURCE	IDENTIFIER
Antibodies		
Anti-phosphotyrosine (pTyr) mouse; PY20	Santa Cruz Biotechnology	PY20
Anti-mouse IgG (H+L) conjugated to Alexa Fluor 647	Thermo/Lifetech	A-21236
His-probe Antibody rabbit (G-18)	Santa Cruz Biotechnology	G-18
Anti-rabbit IgG (H+L) conjugated to Alexa Fluor 680 (used with 700 nm Licor channel)	Thermo/Lifetech	A-21109
IRDye 800CW Goat anti-Mouse IgG (H+L) antibody (used with 800 nm Licor channel)	Licor	925-32210
Bacterial and Virus Strains		
Plasmid propagation: Top10 *E. coli*	Invitrogen	C404010
Protein expression: BL-21 DE3 RIPL	Agilent	230280
Biological Samples		
n/a		
Chemicals, Peptides, and Recombinant Proteins		
DMSO, tissue culture grade (for cell freezing)	Sigma	D2650
Copper (II) sulfate pentahydrate	Sigma	7758-99-9
Actinomycin D	Sigma	50-76-0
15 ml falcon tubes – Cellstar	Greiner	188 271
1.7 ml Eppendorf Tubes	Olympus	24-282
POPC lipid in chloroform	Avanti	850457C
Ni2+-DGS-NTA lipid in chloroform	Avanti	790404C
PEG5000-PE lipid in chloroform	Avanti	880230C
DOPS lipid in chloroform	Avanti	840035C
Atto390-DOPE	ATTO-TEC GmbH	AD 390-161
Atto647-DOPE	ATTO-TECH GmbH	AD 647-161
Rhodamine-PE	Avanti	810150C
Paraformaldehyde	Electron Microscopy Sciences	15712
Triton X-100	Sigma	T8787
Bovine Serum Albumin (BSA)	Sigma	A4737
Hellmanex III	Sigma	Z805939
5N Sodium Hydroxide	Fisher	SS256-500
Rapamycin	Sigma	R0395
Formic Acid (0.1% v/v), mass spec grade	Fisher	LS118-1
Trypsin gold, Mass spectrometry grade	Promega	V5280
Iodoacetamide (IAA)	Sigma	I6125
Bovine Serum Albumin (BSA)	Sigma	A7906
Precission Protease	GE Healthcare	27-0843-01

SNAP-Cell 505-Star	NEB	S9103S
Critical Commercial Assays		
MycoAlert Mycoplasma Detection Kit	Lonza	LT07-318
MycoAlert Mycoplasma Control Set	Lonza	LT07-518
TransIT-Insect	Mirus	MIR 6100
APC Annexin V	BioLegend	640941
Deposited Data		
n/a		
Experimental Models: Cell Lines		
Drosophila S2U Cells	Ron Vale Lab	Flybase ID: FBtc9000006
Experimental Models: Organisms/Strains		
n/a		
Oligonucleotides		
See Supplemental File_Constructs and Oligos, “oligos” tab		
Recombinant DNA		
See Supplemental File_Constructs and Oligos, “constructs” tab		
Software and Algorithms		
GraphPad Prism	GraphPad Software	6.0
Adobe Photoshop	Adobe	CS6
µManager	µManager/Open Imaging	1.4 (updated)
Fiji (is just ImageJ)	Fiji.sc	2.0 (updated)
Other		
Schenider’s Cell Culture Media	Gibco	21720
Fetal Bovie Serum, Heat inactivated	Atlanta	S11150H
Antibiotic-antimycotic	Gibco	15240062
T75 non-vented tissue culture flask	Corning	430720
T25 non-vented tissue culture flask	Corning	430168
Externally threaded cryovials for freezing cells, 2 ml	Corning	430659
Costar TC-treated 6 well plates	Corning	CLS3516
Polystyrene round-bottom tubes (5 ml) for transfection	Falcon	352058
MatriCal Imaging Plates	Brooks	MGB096-1-2-LG-L
Disposable Glass Culture Tubes (lipid mixes)	Fisher	14-961-26
Hamilton Syringes (Gas Tight)	Fisher	8 1100
Tissue Culture Grade PBS	GIbco	20012050

Drierite	Fisher	AC219095000
Bath Sonicator to make SUVs	Diagenode	Pico
Extruder for Liposome Preparation	Avanti	610023
Silica beads for engulfment assay	Bangs Labs	SS06N
Ni-NTA agarose (regenerated)	Qiagen	30210
Glutathione Sepharose (regenerated)	GE Healthcare	17527901
Superdex 200 10/30 GL column	GE Healthcare	17517501
PD Minitrap G-25 column (remove excess BG505 dye)	GE Healthcare	28-9180-07

Figure 1: Cellular reconsitution of Draper signaling

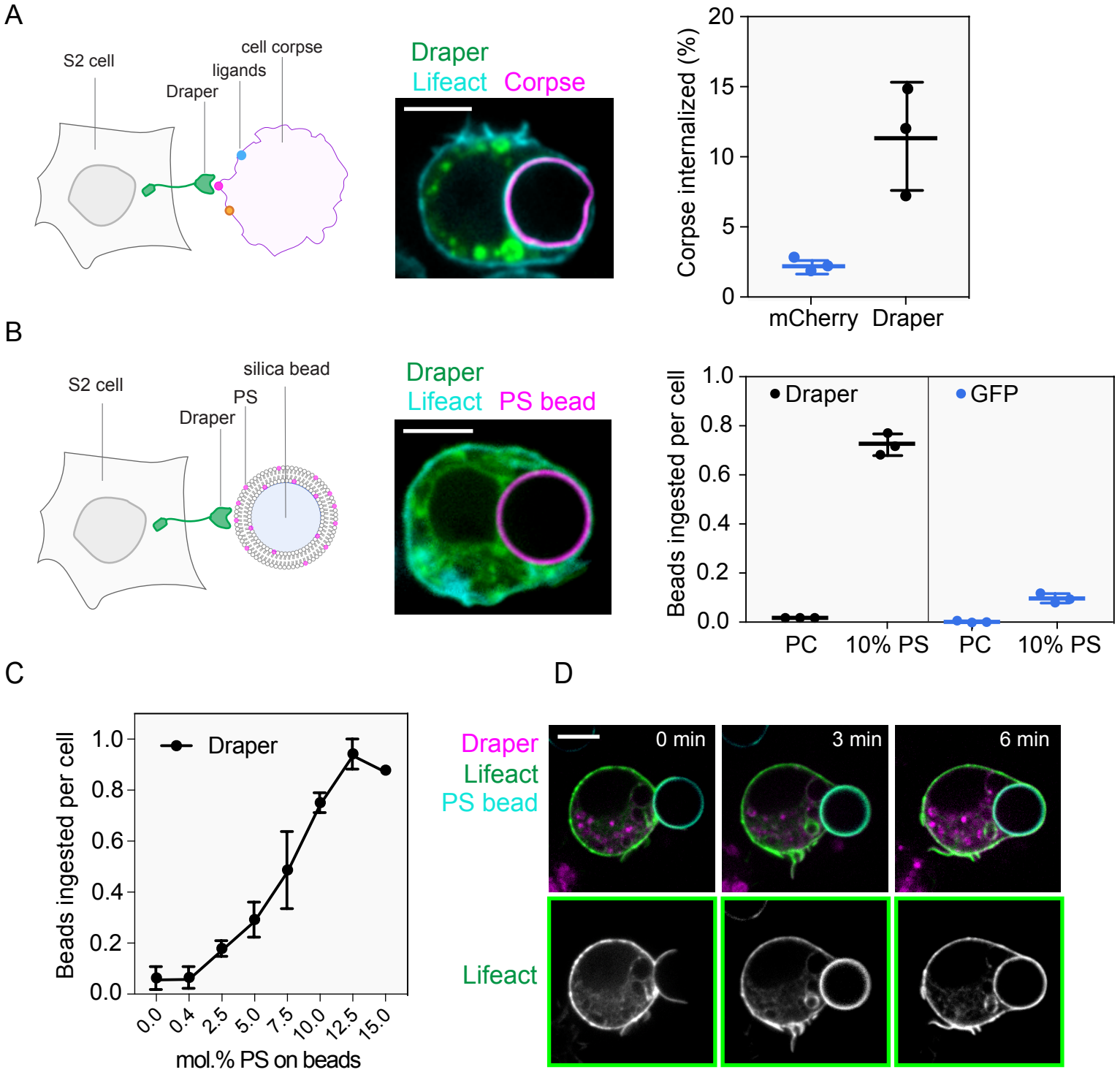

Figure 2: Draper organizes into mobile microclusters that recruit signaling molecules

A

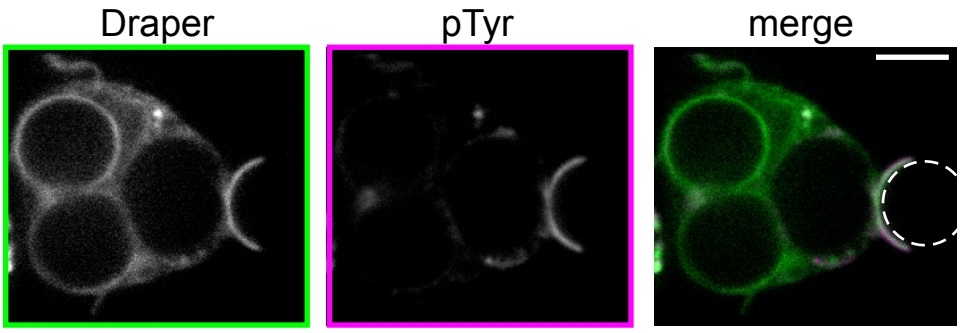

B

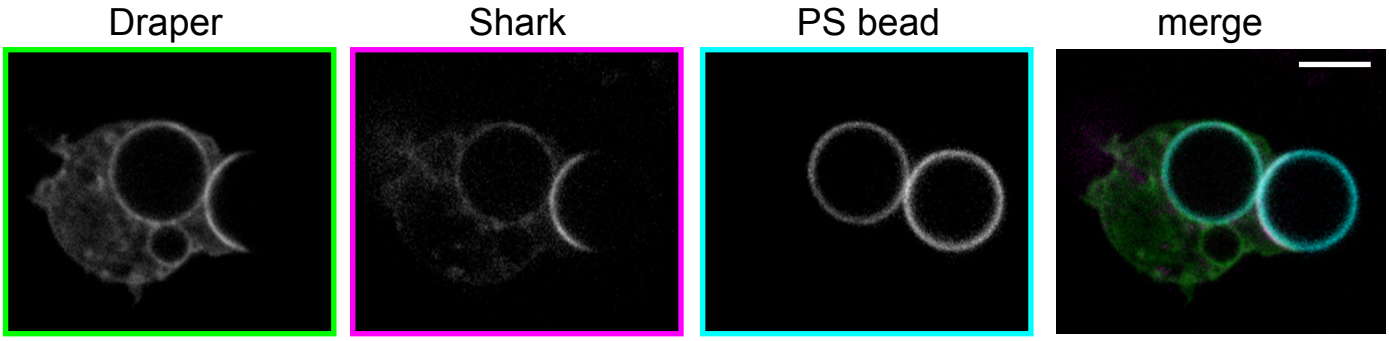

C

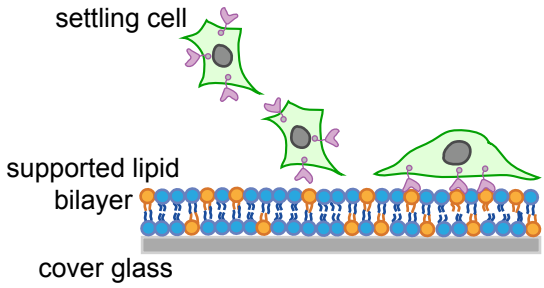

D

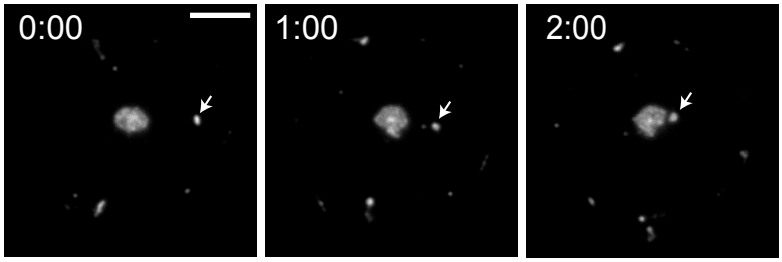

E

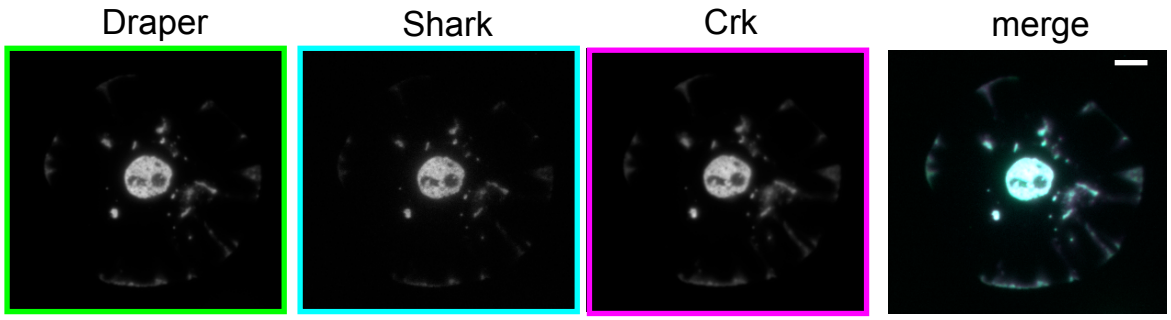

Figure 3: Segregation of Draper and a transmembrane phosphatase at the synapse

A.

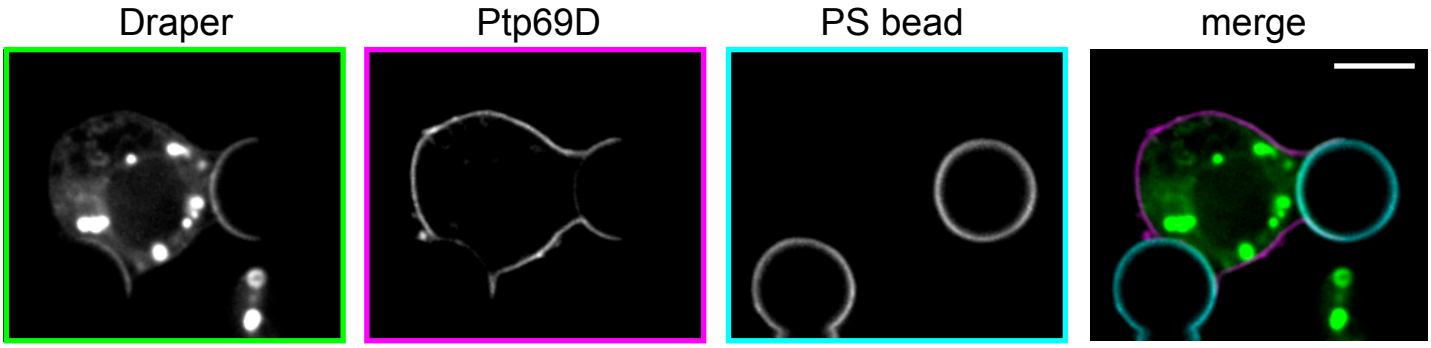

B

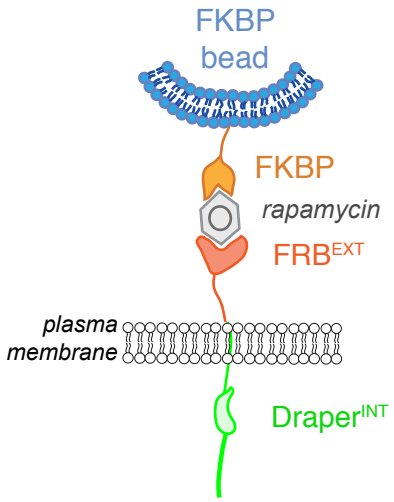

C

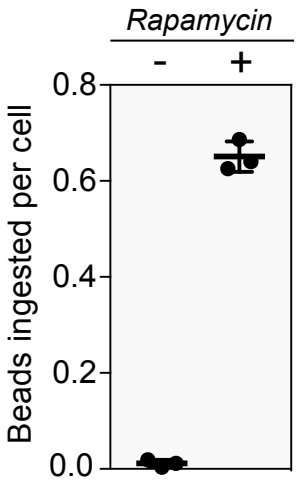

D

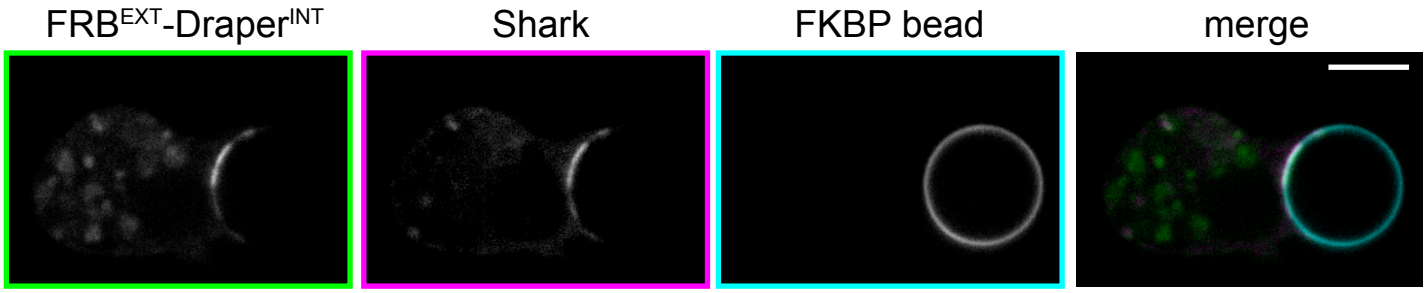

E

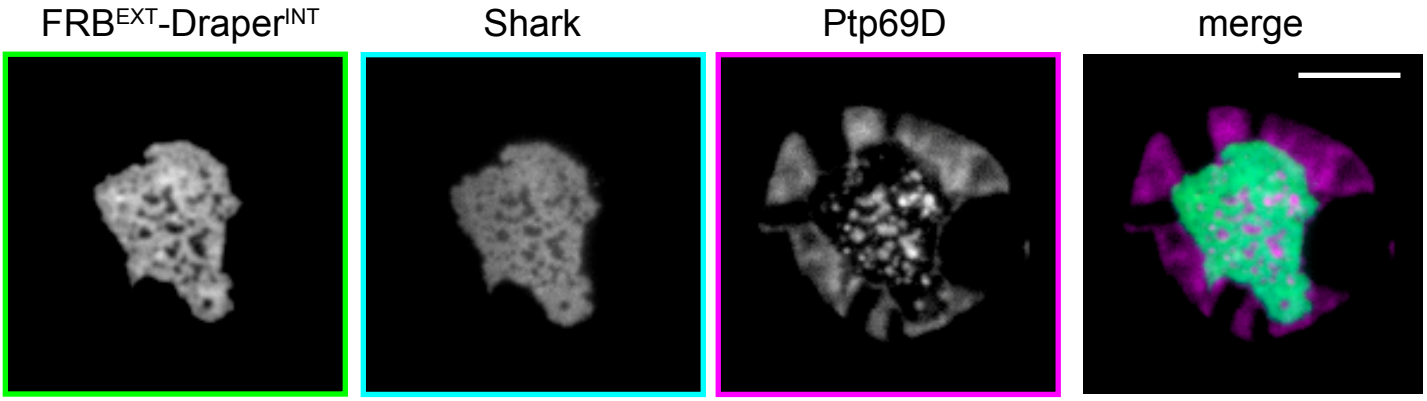

Figure 4: Roles of Draper's cytoplasmic tyrosine residues in engulfment of PS beads

A

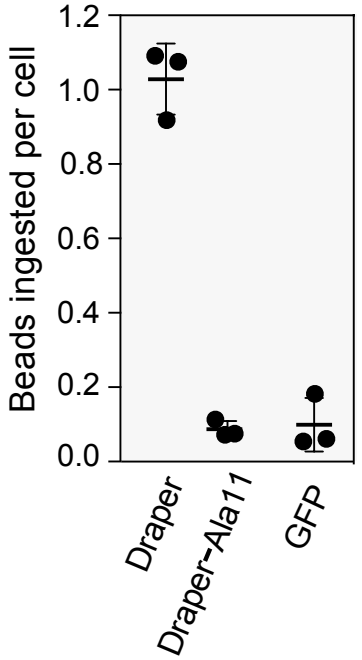

B

C

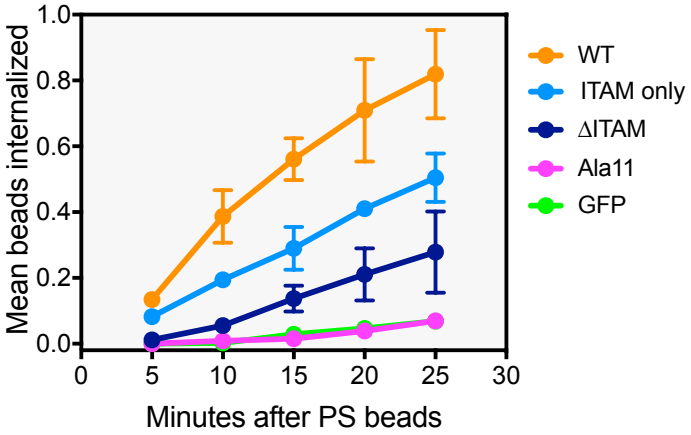

Figure 5: In vitro reconstitution of hierarchical multisite Tyr phosphorylation on Draper

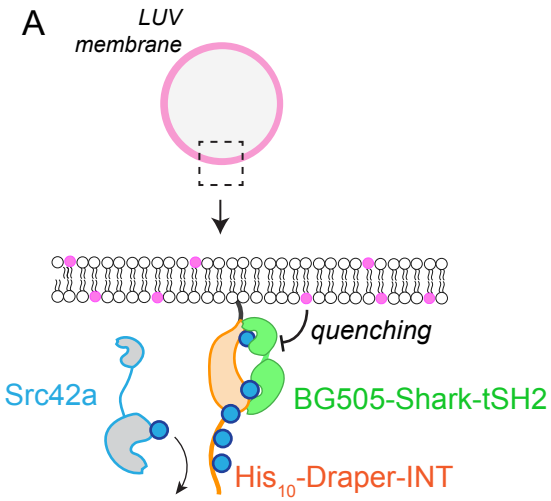

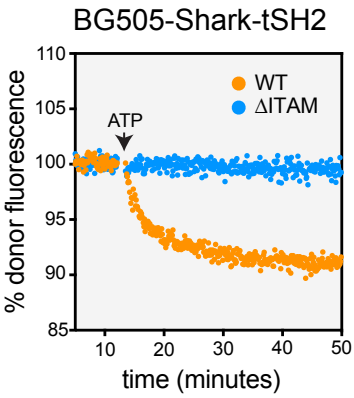

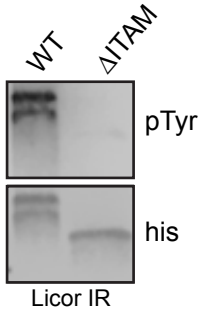

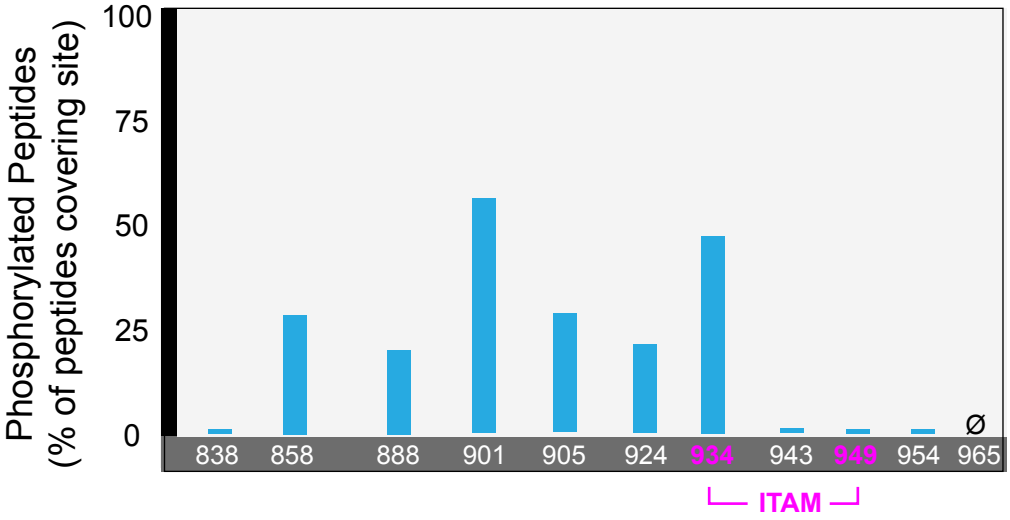

Figure 6: Mechanism of Draper triggering

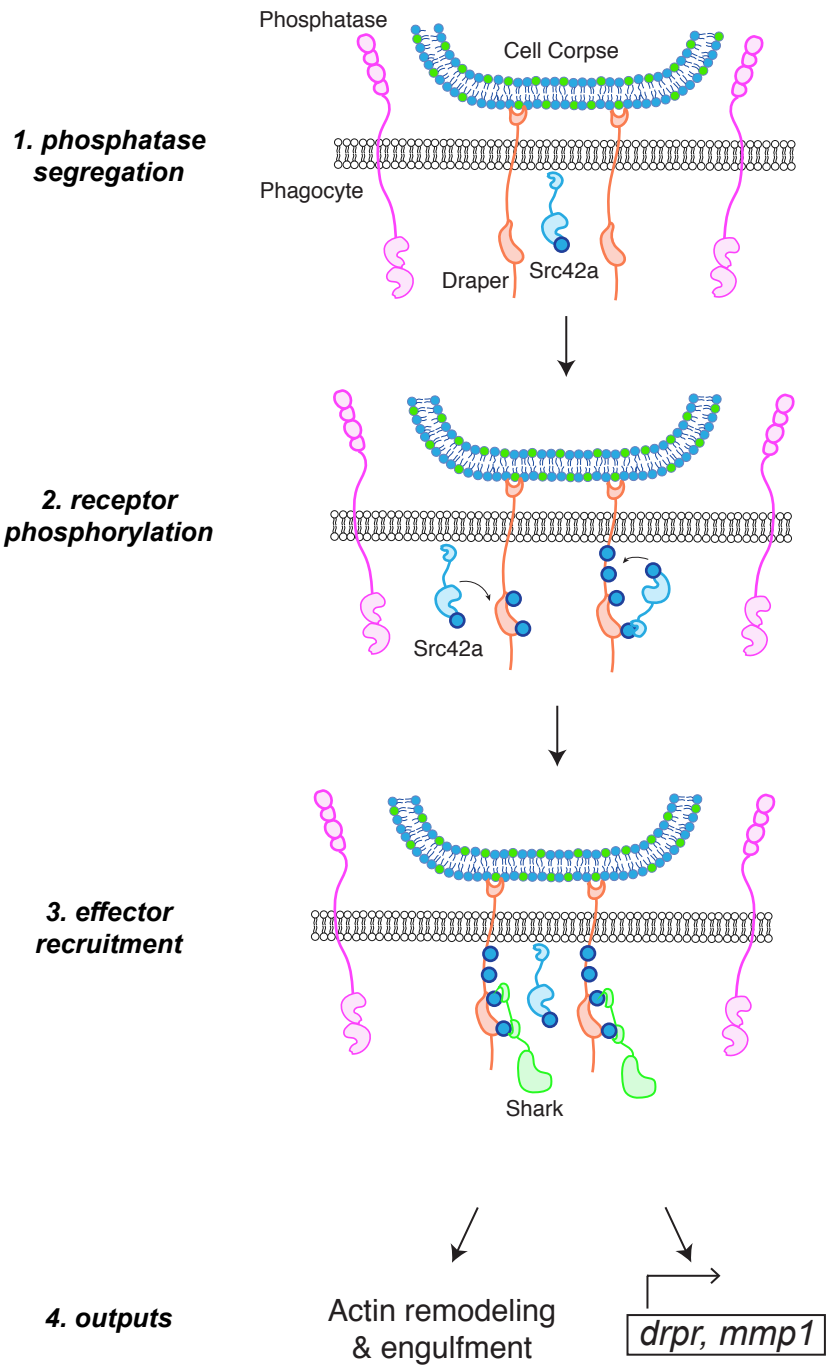

Figure S1 (related to Figure 2): p85 and Crk are recruited to the synapse with a 10% PS bead

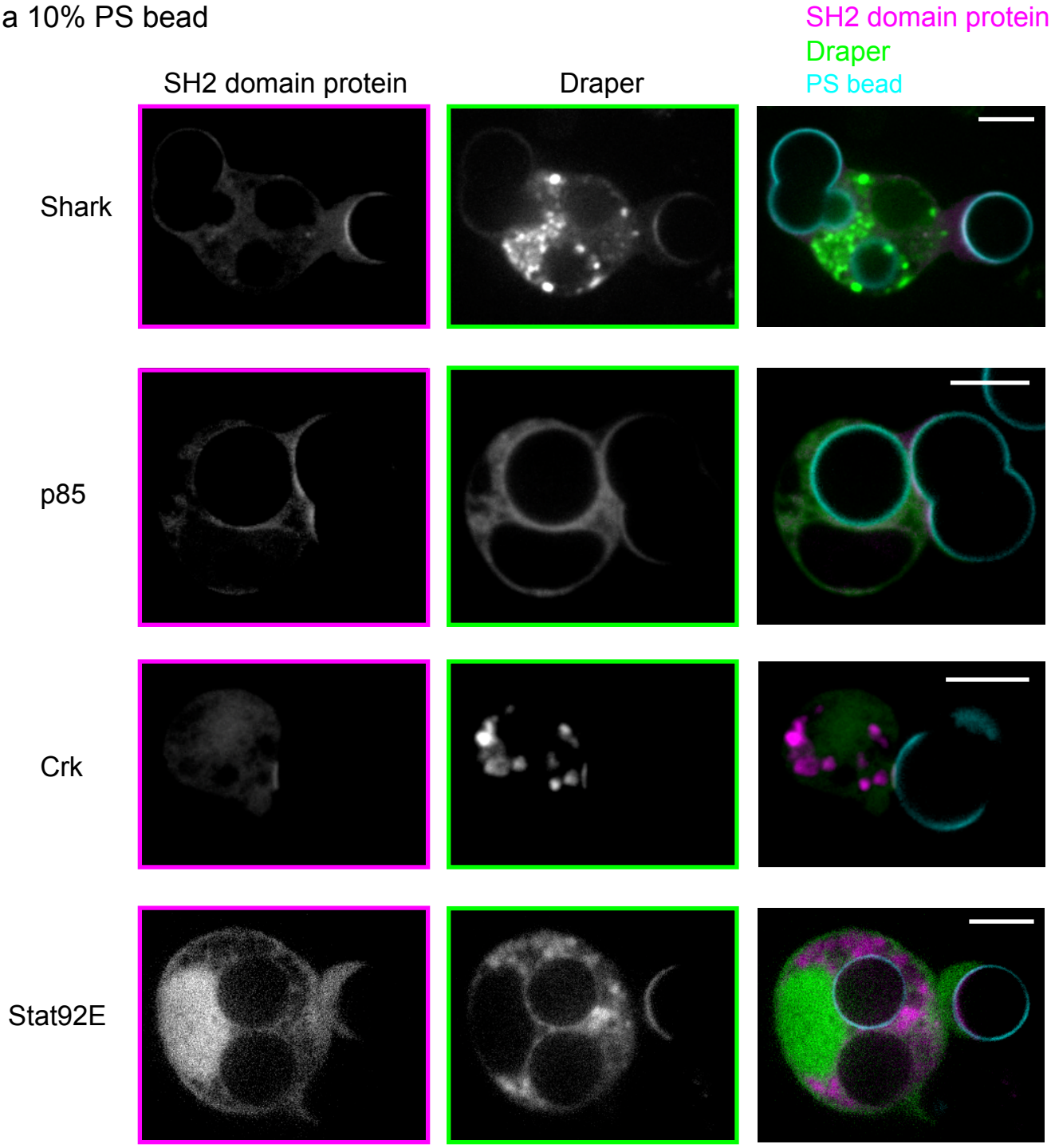

Figure S2 (related to Figure 3): The transmembrane phosphatase Ptp69D

A

Phosphatase	RPKM
Ptp4E	25.87
Ptp69D	21.82
l(1)G0232	16.56
Ptp10D	11.23
CG12746	10.54
Lar	10.10
Ptp99A	7.89

B

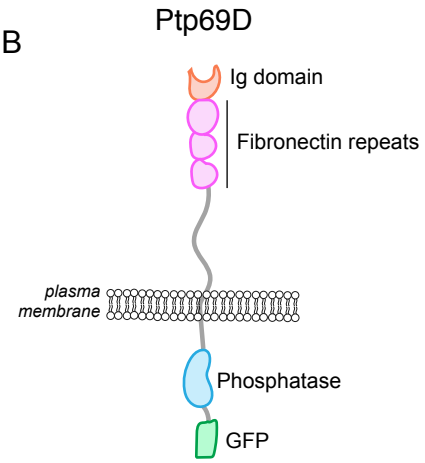

C

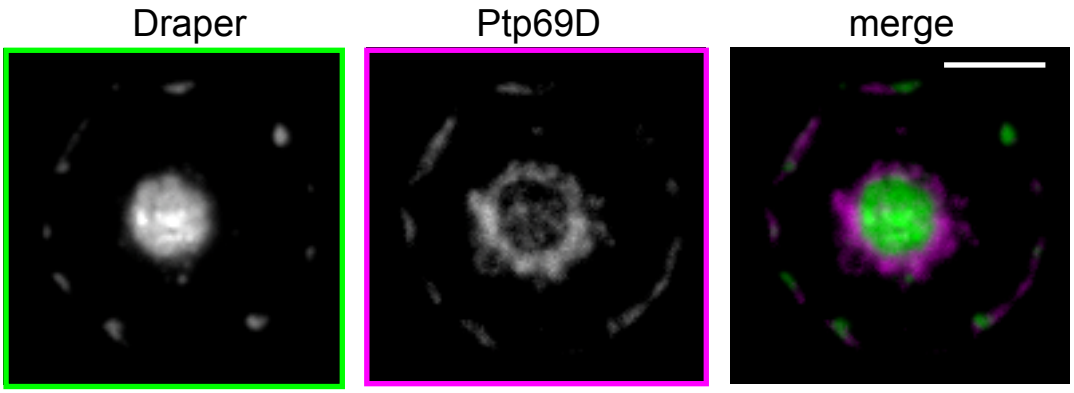

Figure S3 (related to Figure 4): Draper's ITAM is necessary and sufficient to recruit Shark in cells

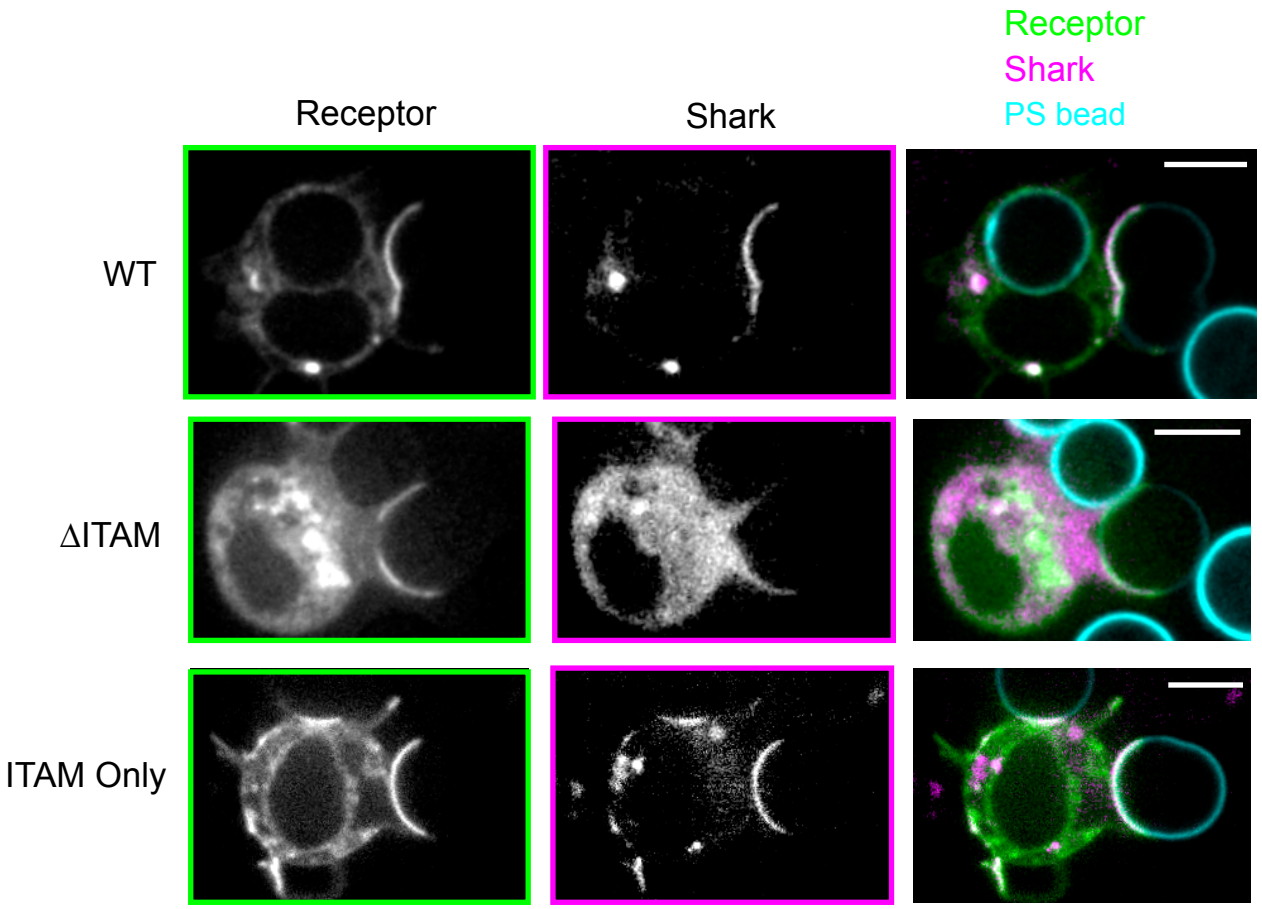
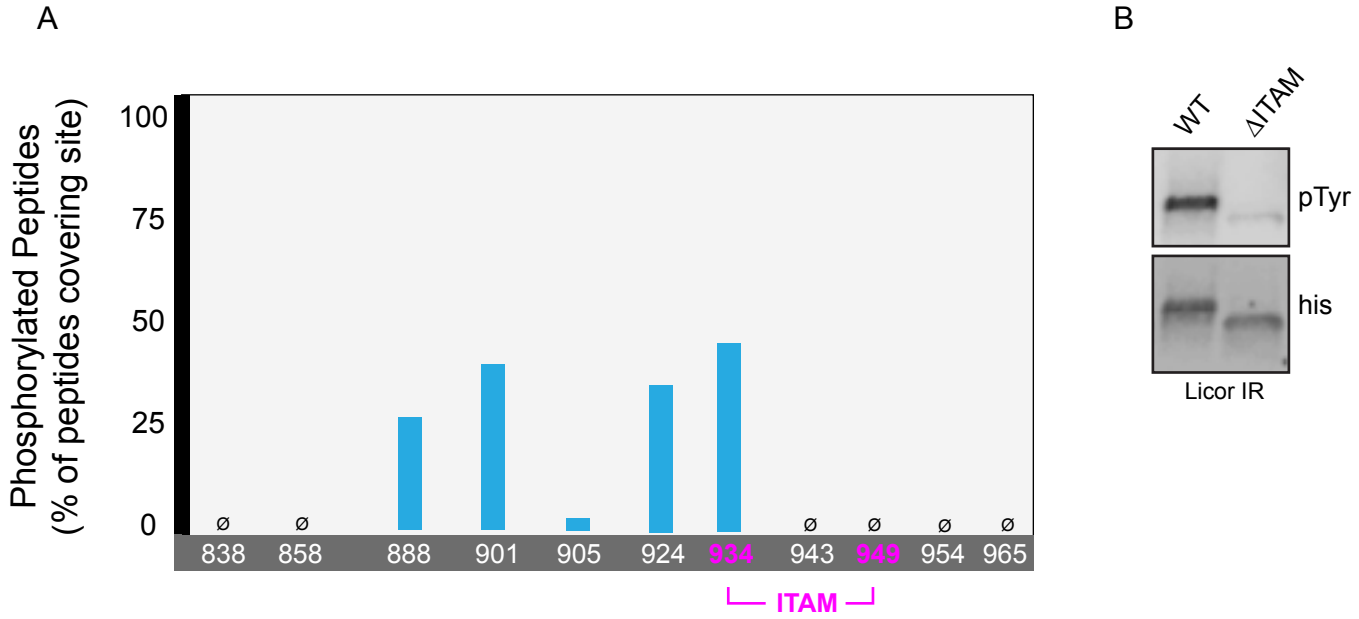
Figure S4 (related to Figure 5): Identification of phosphorylation sites on Draper by Lck